

## ABSTRACT

Title of Document:                   ENERGETICALLY AUTONOMOUS  
  TACTICAL ROBOTS

Elias Zeilah, Mechanical Engineering, 2012

Directed By:                         Dr. Bilal M. Ayyub, Department of Civil and  
  Environmental Engineering

Autonomous vehicle research has been on the rise in recent years. The need for autonomous vehicles and functions is growing for both everyday driving and military use. Current techniques have been shown to adequately navigate vehicles around a closed course. However, in hostile situations, where the objective timeframe is unclear, an autonomous vehicle alone would not be reliable in carrying out a mission. In this work, a system capable of both recognizing and acquiring biomass for self-fueling is investigated. Incorporating such a system with an autonomous vehicle would allow for a self-sustaining vehicle capable of being sent on a mission indefinitely. A study is done on the feasibility and requirements of a fully integrated system. It has been shown that the system is able to accurately distinguish and obtain a biomass source in a multi object environment. This biomass is then sent to an engine for burning and conversion to electrical energy. The energy is then stored in a system of batteries and used to sustain the operation of the platform.

ENERGETICALLY AUTONOMOUS TACTICAL ROBOTS

By

Elias Zeilah

Thesis submitted to the Faculty of the Graduate School of the  
University of Maryland, College Park, in partial fulfillment  
of the requirements for the degree of  
Masters of Science  
2012

Advisory Committee:  
Professor Bilal Ayyub, Chair  
Professor Bao Yang  
Professor Guangming Zhang

© Copyright by  
Elias Zeilah  
2012

## **Dedication**

I dedicate this to my friends and family.

## **Acknowledgements**

First and foremost I would like to thank my advisor, Professor Bilal Ayyub. I am very appreciative of the opportunity and guidance he has given me over the years. I would also like to thank Dr. Robert Finkelstein and Robotic Technology, Inc., Nikolay Tikhonov, Cheyu Cheng, Clara Popescu and the remainder of the EATR group for their support on this project.

Finally I would like to thank my family and friends who have always been there to lend a helping hand and support me through everything.

# Table of Contents

<b>Dedication</b> .....	ii
<b>Acknowledgements</b> .....	iii
<b>Table of Contents</b> .....	iv
<b>List of Tables</b> .....	vii
<b>List of Figures</b> .....	viii
<b>Chapter 1: Introduction</b> .....	1
1.1. Motivation.....	1
1.1.1. Surveillance and reconnaissance.....	1
1.1.2. Need for unmanned vehicles.....	1
1.2. Current projects involving autonomous control .....	2
1.2.1. DARPA grand challenge.....	2
1.2.2. Unmanned aerial vehicles.....	3
<b>Chapter 2: EATR system overview</b> .....	7
2.1 Objective.....	7
2.2 System overview.....	7
2.2.1 Sensory system.....	7
2.2.2 Energy system.....	8
2.2.3 Control system .....	9
2.2.4 Energy harvesting .....	9
2.2.5 Battery comparisons.....	12
<b>Chapter 3: Sensory system</b> .....	14
3.1 Introduction.....	14
3.2 Components .....	15
3.2.1 Ladar .....	15
3.2.2 Video Camera .....	19
3.2.3 Robot Arm .....	21
3.2.4 Relative humidity (RH) sensor .....	25
3.2.5 Oxygen sensor.....	26
3.2.6 Arduino UNO.....	27
<b>Chapter 4: Energy system</b> .....	29
4.1 Introduction.....	29
4.2 Cyclone engine components .....	30
4.2.1 Hopper and feeder.....	30

4.2.2 Burner .....	30
4.2.3 Heat exchanger.....	31
4.2.4 Waste heat engine .....	31
4.2.5 Condenser system .....	32
4.2.6 Alternator .....	33
4.2.7 Engine illustration and setup.....	34
4.3 Wood chipper.....	35
4.4 Battery Setup.....	38
4.5 Integration .....	39
4.6 Pellx controller.....	40
<b>Chapter 5: System Integration .....</b>	<b>48</b>
5.1 Introduction.....	48
5.2 Sensory system integration .....	48
5.2.1 Mounting the system components .....	48
5.2.2 Connecting the system components.....	48
5.3 Energy system integration.....	50
5.4 Control system integration.....	50
5.4.1 Pellx controller adapter .....	50
5.4.2 Fuel moisture content monitor .....	54
<b>Chapter 6: Results.....</b>	<b>59</b>
6.1 Introduction.....	59
6.2 LADAR results .....	59
6.2.1 Hokuyo software.....	59
6.2.2 Integrated with MATLAB .....	60
6.3 LADAR and webcam results .....	63
6.3.1 Single object target .....	63
6.3.2 Multi object target.....	66
6.3.3 Watershed method for multiple objects .....	66
6.4 Determining inverse kinematics .....	70
6.4.1 Inverse Kinematics calculation for a single object .....	70
6.4.2 Inverse kinematics calculation for two objects.....	73
6.4.3 Inverse kinematics for multiple objects .....	76
6.5 Distinguishing between biomass.....	78
6.5.1 Controlled environment .....	78
6.5.2 Real environment.....	83
<b>Chapter 7: Conclusions .....</b>	<b>89</b>
<b>Chapter 8: Future Work .....</b>	<b>90</b>
<b>Bibliography .....</b>	<b>91</b>





## **List of Tables**

Table 2.1 List of required devices.....	8
Table 2.2 Power consumption of the system .....	9
Table 2.3 Comparison of various batteries .....	12
Table 4.1 Chipping capacity vs. power required .....	36

## List of Figures

Figure 1.1 Red Bull autonomous vehicle for DARPA Grand Challenge (1).....	2
Figure 1.2 Combination of sensors used for autonomous detection of the terrain (1)..	3
Figure 1.3 DARPA grand challenge terrain (left). Terrain after image processing (right) (1).....	3
Figure 1.4 UAV communication systems (2) .....	4
Figure 1.5 UAV system components (3) .....	6
Figure 2.1 Energy content for various biomass sources (6).....	12
Figure 3.1 Sensory system criteria.....	14
Figure 3.2 Ladar system (8).....	15
Figure 3.3 Photons in the LADAR path (8).....	17
Figure 3.4 The additive model of RGB. Red, green and blue are the primary stimuli for the human color perception and are the primary additive colors (9). .....	20
Figure 3.5 Robot arm with degrees of freedom .....	22
Figure 3.6 The robot arm at rest.....	22
Figure 3.7 Wheatstone bridge .....	23
Figure 3.8 Schematic of an RH sensor (13).....	25
Figure 3.9 Diagram of an O <sub>2</sub> sensor (14).....	26
Figure 3.10 V <sub>out</sub> vs air/fuel ratio for an O <sub>2</sub> sensor (14).....	27
Figure 3.11 Arduino board (15).....	28
Figure 4.1 Energy system criteria .....	29
Figure 4.2 Heat exchanger of the cyclone engine (16) .....	31
Figure 4.3 Major inlet and outlet connections for cyclone waste heat engine (16)...	32
Figure 4.4 Condenser fans (16).....	33
Figure 4.5 Alternator output (16).....	34
Figure 4.6 Schematic of cyclone engine .....	34
Figure 4.7 Plot of chipping capacity vs. power required .....	37
Figure 4.8 Wood chipper design and placement.....	38
Figure 4.9 Battery setup.....	39
Figure 4.10 Interface between battery outputs and sensors .....	40
Figure 4.11 Pellx controller (20).....	41
Figure 4.12 Schematic of the control box (16) .....	46
Figure 5.1 Robot arm with attached sensors.....	49
Figure 5.2 Connecting the energy system to the sensors .....	50
Figure 5.3 O <sub>2</sub> /fan controller .....	53
Figure 5.4 RH monitor and controller.....	55
Figure 5.5 Side view of the storage canister lid.....	58
Figure 5.6 Storage canister with dehumidifying system.....	58
Figure 5.7 Side view of fan setup .....	58
Figure 6.1 LADAR output (25) .....	60
Figure 6.2 Target area to be examined (25).....	61
Figure 6.3 3D representation of the target area (25).....	61
Figure 6.4 Inverse of the 3D image (25).....	62
Figure 6.5 Reverse of the 3D image (25).....	62
Figure 6.6 Motions of the robot arm for target frame (25) .....	63

Figure 6.7 Image of scanned tennis ball (25).....	64
Figure 6.8 Adjusted scale for tennis ball representation (25) .....	65
Figure 6.9 3D representation of tennis ball (25).....	65
Figure 6.10 Multi object capture of target area (25).....	66
Figure 6.11 Step 1 taking the gradient magnitude (25) .....	67
Figure 6.12 Step 2 segmenting the image using the watershed transformation (25)..	67
Figure 6.13 Step 3 transparently superimposing Lrgb on the original image (25).....	68
Figure 6.14 Step 4 cleaning up the selected color segments (25).....	68
Figure 6.15 Step 5 of determination of the centroids watershed approach (25) .....	69
Figure 6.16 Step 6 calculating the k values (25).....	69
Figure 6.17 Tennis ball to be captured (25).....	70
Figure 6.18 Ladar image of tennis ball (25) .....	71
Figure 6.19 3D image of tennis ball (25).....	71
Figure 6.20 Before elimination of the very small files (25) .....	72
Figure 6.21 Distinguishing between objects to find the centroid (25).....	73
Figure 6.22 LADAR result for multiple objects (25) .....	74
Figure 6.23 3D representation for multiple objects (25).....	74
Figure 6.24 Representation after eliminating the very small objects (25).....	75
Figure 6.25 Centroid calculation for multiple objects (25).....	75
Figure 6.26 LADAR scan for multiple objects (25) .....	76
Figure 6.27 3D representation of target area (25).....	76
Figure 6.28 Image with the very small files attached (25) .....	77
Figure 6.29 Image after eliminating the very small files (25) .....	77
Figure 6.30 Test area for biomass distinction (25) .....	78
Figure 6.31 LADAR representation of the results (25) .....	79
Figure 6.32 Side view of the target area (25).....	79
Figure 6.33 Gradient magnitude of the image (25).....	80
Figure 6.34 Image after “opening-by-reconstruction” and “closing-by-reconstruction” techniques (25).....	81
Figure 6.35 Comparison of threshold “opening/closing-by-reconstruction” (25).....	81
Figure 6.36 Finding the k factors of the objects (25).....	83
Figure 6.37 Real environment target area (25) .....	83
Figure 6.38 Centroid calculation for the various objects in the target area (25) .....	84
Figure 6.39 K factor calculation of the target area (25).....	84
Figure 6.40 The second real scene target area (25) .....	85
Figure 6.41 Gradient magnitude of the target area (25).....	86
Figure 6.42 Filtering the gradient magnitude (25).....	86
Figure 6.43 Watershed segmentation (25).....	87
Figure 6.44 Calculating the k factors for the various objects (25).....	87

# Chapter 1: Introduction

## 1.1. Motivation

### 1.1.1. Surveillance and reconnaissance

Reconnaissance, surveillance, and intelligence have long been one of the most important military operations. This process involves acquiring, monitoring and analyzing possible sources of threats. Ever since the surprise attacks of Pearl Harbor, by the Japanese, military surveillance has been continuously evolving to anticipate early threats by hostile forces. The first successful satellite reconnaissance mission took place on August 1960 where satellite footage was taken of the USSR and China. Since then the technology involved in reconnaissance has evolved. In addition to satellite surveillance, uninhabited aerial vehicles (UAV's) are now being used to monitor potential threats.

### 1.1.2. Need for unmanned vehicles

In a war zone, it is important to conduct intelligence, surveillance and reconnaissance missions. In a growing effort to keep casualties down without compromising the effectiveness of the mission a growing need for stealth unmanned vehicles is essential.

One of the current major downfalls of the unmanned systems is the restriction on the mission time due to the limited energy source. With the energetically autonomous tactical robot (EATR), once the power source nears depletion, a signal is sent to the

energy system to combust more fuel and scan the environment for potential biomass to recharge the batteries as needed.

## 1.2. Current projects involving autonomous control

### 1.2.1. DARPA grand challenge

The DARPA grand challenge was the first practical application of autonomous vehicle research in the world. One of the more recent challenges, which took place in 2007, involved a closed sixty mile urban area course. Along with completing the course in less than six hours, the autonomous vehicle is required to obey all traffic regulations along with communicating with other traffic, obstacles and merging into oncoming traffic.



**Figure 1.1 Red Bull autonomous vehicle for DARPA Grand Challenge (1)**

The technology used by the various teams included LADAR's, SONAR's, laptops and various programming languages. The teams use various image processing techniques to analyze the incoming data and interpret the terrain.

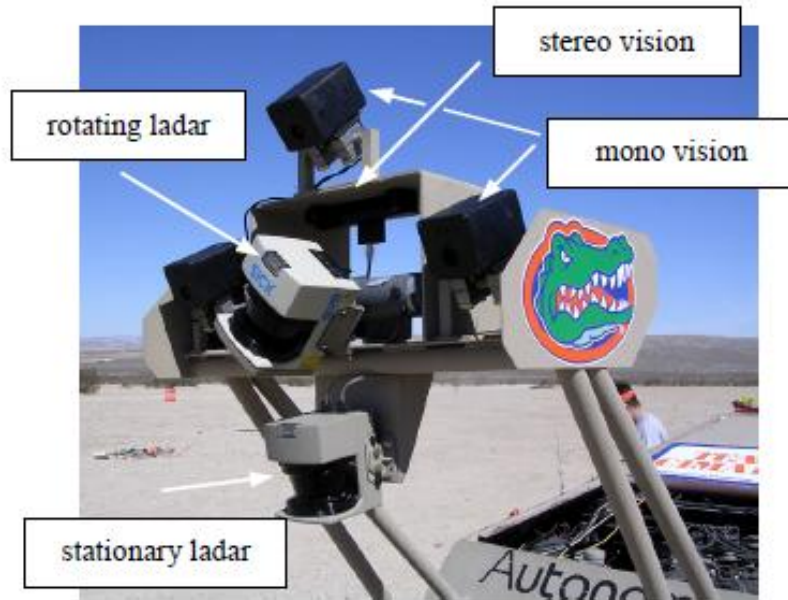


**Figure 1.2 Combination of sensors used for autonomous detection of the terrain (1)**

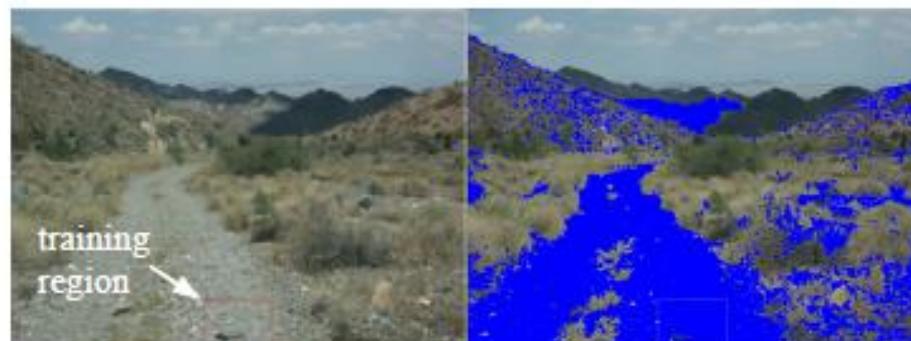


**Figure 1.3 DARPA grand challenge terrain (left). Terrain after image processing (right) (1)**

Combining these various sensors and processing the data allows for assessment and maneuvering of the course (1).

### 1.2.2. Unmanned aerial vehicles

UAV's are remotely controlled, semi-autonomous aerial vehicles that are capable of performing sophisticated reconnaissance missions. The predator UAV can be programmed to run autonomously to execute a simple mission or can be controlled, by a pilot and sensor operator, from the ground control station.

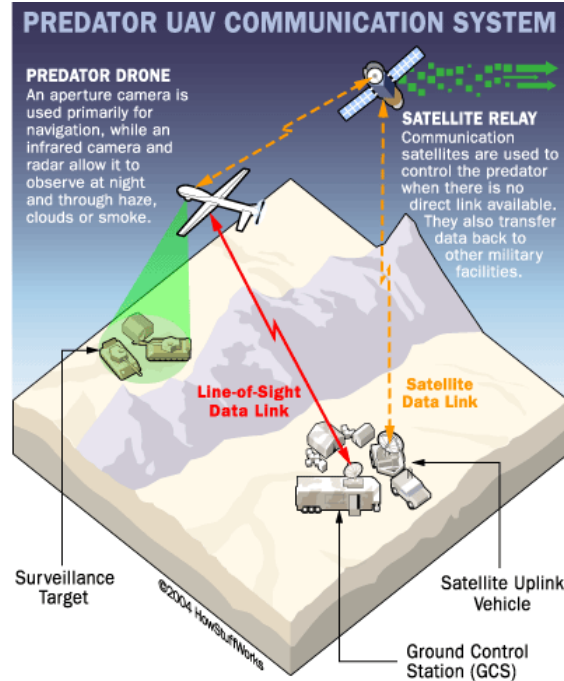


**Figure 1.4 UAV communication systems (2)**

There are various components and sensors involved in the overall system acquisition.

These components and sensors consist of:

1. Synthetic Aperture Radar (SAR) Antenna
2. Inertial Navigation System/GPS
3. Ku-Band Satellite Communications Antenna
4. Video Cassette Recorder
5. GPS Antennas (Left and Right)
6. APX-100 Identification Friend or Foe Transponder
7. Ku-Band Satellite Communications Sensor Processor Modem Assembly
8. C-Band Upper Omnidirectional Antenna Bracket
9. Forward Fuel Cell Assembly

10. Aft Fuel Cell Assembly
11. Accessory Bay
12. Engine Cooling Fan
13. Oil Cooler/Radiator
14. 914F Engine
15. Tail Servo (Left and Right)
16. Battery Assembly #2
17. Power Supply
18. Battery Assembly #1
19. Aft Equipment Bay Tray
20. Secondary Control Module
21. Synthetic Aperture Radar Processor/AGM-114 Electronics Assembly
22. Primary Control Module
23. Front Bay Avionics Tray
24. ARC-210 Receiver/Transmitter
25. Flight Sensor Unit
26. Video Encoder
27. De-ice Controller
28. Electro-Optical/Infrared Sensor/AN/AAS-52(V)1 Electronics Assembly
29. Front Bay Payload Tray
30. Ice Detector
31. Synthetic Aperture Radar (SAR) Receiver/Transmitter
32. Nose Camera Assembly



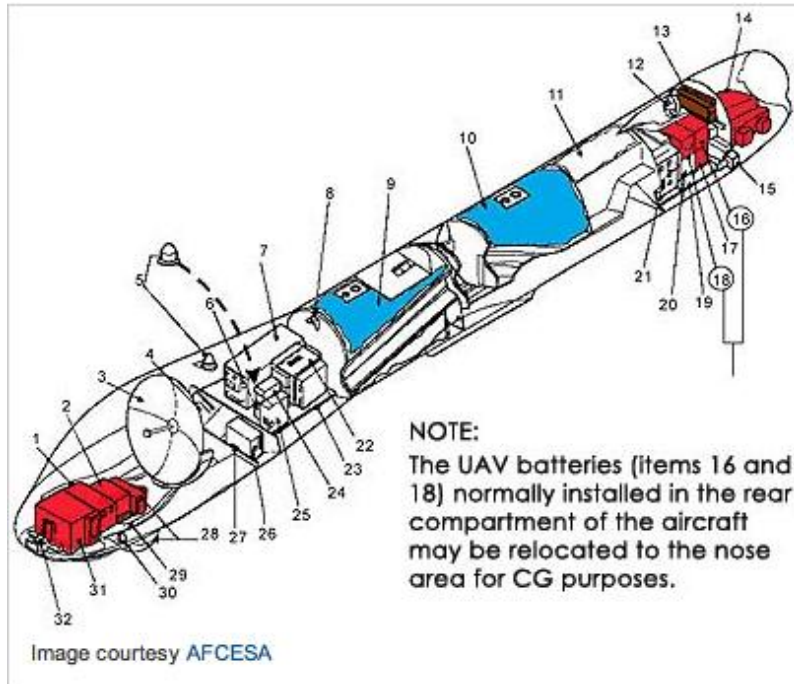


**Figure 1.5 UAV system components (3)**

In order to capture advanced imaging under various conditions, sophisticated monitoring equipment is used. A variable aperture camera is used as the UAV's main set of eyes. The addition of a variable aperture infrared camera allows for low-light and night imaging. Similarly, the synthetic aperture radar is essential to see through fog or smoke. The combination of all these sensors allows for the end user to adequately assess the end picture seen by the UAV (4).

## **Chapter 2: EATR system overview**

### 2.1 Objective

The energetically autonomous tactical robot's (EATR) overall objective is to perform surveillance missions without the aid of human control. Rendering the use of a sensory and electronics system, the EATR will be able to navigate terrain and avoid obstacles to reach a specific destination. During the mission, the EATR will scan the terrain in search of combustible biomass, which will be used to fuel a cyclone steam engine. Thus engine will then charge a system of batteries used to run both the vehicle and the sensory system. The charge in the batteries will be monitored and recharged accordingly. When the system needs to be recharged the EATR will pause the mission and scan the environment for biomass. Biomass will be distinguished using both the sensory system and image processing. This system can be used in high-risk surveillance missions so not to jeopardize the life of soldiers.

The scope of this project consists of designing a system capable of detecting and acquiring biomass as a means for fuel. The system can be broken down into multiple subsystems, mainly the sensory, energy and control systems.

### 2.2 System overview

#### 2.2.1 Sensory system

The sensory system will be composed of a series of sensors capable of measuring distance and weight in addition to video monitoring hardware needed for image processing. The following table summarizes the sensors to be used along with the

function of each.

Device	Purpose	Specifications	Cost
Ladar	Measures the distance between the robot arm and the object it will grasp	240° with 20 to 5,600 mm detection range and 28 msec/scan, scan time	\$2,800
Video Camera	Scans the environment for potential biomass	Capable of capturing images within 5m	\$235
Webcam	Takes images of a target object once the video camera selects the target	USB 2.0 compatible	\$70
Pan tilt	Used as a mount for the video	Capable of maneuvering the payload of the camera	\$2100
Laptop	Analyzes the information and outputs a response	Quad core	\$1200
Robot Arm	Picks up the target biomass	6 degrees of freedom	\$20,000
USB Hub	Allows multiple USB connections to the laptop	USB 2.0	\$40
Strain Gauge	Capable of measuring weight and pressure	Easily mountable on the arm	\$8
Arduino electronics prototyping platform	Used to output a command based on a given input	Arduino UNO	\$40
20 Huamo HM12-50 Batteries	Supply power to the system while engine is not charging	12V 50AH batteries	\$1,300
BZ MPPT500HV charge controller	Monitors battery charging and discharging	24V, 500 W input	\$195
HS-2000 RH sensor	Monitors temperature and relative humidity in the system	+/- 2%RH	\$40
Koso narrow band O <sub>2</sub> sensor	Monitors the air/fuel ratio of the exhaust gas	0.2V-9V range	\$57
			\$28,085

**Table 2.1 List of required devices**

### 2.2.2 Energy system

In order for the system to be able to sustain autonomous power in most environments, a biomass fuel source was chosen since this can be readily found in a majority of the

environments. To convert the biomass fuel to useable energy, the source must be burned and the heat converted to electricity. The overall power is found by summing the total power of the system components.

Device	Voltage (V)	Current (A)	Power (W)
Ladar	12	0.375	4.5
Laptop	19.5	4.62	90.09
Video Camera (big)	15	0.5	7.5
Pan Tilt	24	4.3	129
Robot Arm	24	10	240
USB Hub	5	3.8	19
Arduino UNO	5	0.5	2.5
Strain gauge, O <sub>2</sub> , and RH sensor	5	< 0.1	< 1
			466.78

**Table 2.2 Power consumption of the system**

A total power of 470 watts is needed to power the system.

### 2.2.3 Control system

The system must be equipped with a control architecture capable of analyzing the incoming information, from the sensory system, and providing an adequate output.

This will be done using a combination of microcontrollers and a laptop processor (along with the accompanied software).

### 2.2.4 Energy harvesting

Energy is defined as the ability of a product to do work. There are various types of energy including: kinetic, potential, thermal, sound, light, and electromagnetic. It is

possible to transform any of the types of energies into another, however there is a conversion efficiency associated with this transformation, which yields a certain loss. In order to maximize the remaining energy from a conversion, the most efficient method would be sought. For the purpose of the EATR, a conversion from thermal into electrical energy is of interest.

Power is defined as the rate at which work is performed or energy converted. The average power is given by:

$$P_{avg} = \frac{\Delta W}{\Delta t}$$

2.1

Where  $\Delta W$  is the amount of work performed and  $\Delta t$  is the amount of time. When the rate of energy transfer is constant this can be simplified to:

$$P = \frac{W}{t} = \frac{E}{t}$$

2.2

Where  $W$  is the work done and  $E$  is the energy transferred.

From table 2, 470 watts is needed to power the EATR system. Assuming the system needs to run for a day, 86400 seconds, without the need to recharge, the amount of energy can be calculated.

$$E = Pt$$

2.3

$$E = (470 \text{ W})(86400 \text{ s}) = 40.6 \text{ MJ}$$

A total of 40.6 mega joules are needed to power the 470W EATR system for a 24 hour period.

$$1 \text{ Kilowatt hour (KWh)} = 3.6 \text{ mega joules}$$

$$(40.6 \text{ mega joules} / 3.6 \text{ mega joules}) 1 \text{ KWh} = 11.278 \text{ KWh}$$

Energy harvesting, from a biomass source, is an environment dependent task. The amount of biomass the EATR will need to harvest will depend on the potential energy available in the biomass of that environment. The energy content is dependent on properties such as density and condition (wet, dry, or seasoned) of the fuel. In order to understand the amount of biomass needed to achieve an 11.3 KWh goal. A study was done on various species of wood pellets, using a bomb calorimeter, to determine their heating values. The heating value is the amount of heat produced by the combustion of a unit quantity of fuel. If the products of combustion remain in the gaseous state then the heat given off during combustion is classified as the low heating value (LHV). However, in the bomb calorimeter, the products of combustion are cooled to the temperature of the original gas & air mixture. When this cooling takes place the water produced during combustion condenses and the heat of condensation is added to the low heat value. This results in the high heating value (HHV) (5). Table shows some values of common species of wood. The LHV is of interest since this value is achievable outside of an experimental setting. From the table below it can be seen that a LHV of at least 14.41 MJ/Kg is achievable with moisture content of 11.5%. Assuming a 30% efficiency of the EATR engine, this yields a power output of 4.323 MJ/Kg or 1.2 KWh/Kg (6).

Sample	Species	HHV (kJ/kg)	LHV (kJ/kg)	M <sub>ar</sub> (%)
P4	<i>Pinus pinaster</i>	20237.89 ± 374.12 (1.849)	16935.72 ± 335.46 (1.981)	10.3
P8	<i>Pseudotsuga menziesii</i>	19660.02 ± 32.29 (0.164)	16704.30 ± 29.46 (0.176)	8.8
P12	<i>Cedrus atlantica</i>	20360.45 ± 187.30 (0.920)	15629.71 ± 154.00 (0.985)	17.8
P1	<i>Castanea sativa</i>	18754.86 ± 218.64 (1.166)	15468.56 ± 194.33 (1.256)	11.1
P2	<i>Eucalyptus globulus</i>	17631.66 ± 326.53 (1.852)	14411.54 ± 289.03 (2.006)	11.5
P3	<i>Fagus sylvatica</i>	19132.47 ± 231.97 (1.212)	15818.67 ± 206.36 (1.304)	11.0
P5	<i>Quercus robur</i>	18696.82 ± 47.00 (0.251)	15361.13 ± 41.63 (0.271)	11.4
P6	<i>Fraxinus angustifolia</i>	19090.90 ± 306.18 (1.604)	16450.82 ± 283.92 (1.726)	7.3
P7	<i>Prunus avium</i>	18256.48 ± 120.86 (0.662)	15552.33 ± 111.18 (0.715)	8.0
P9	<i>Salix babylonica</i>	18279.41 ± 348.08 (1.904)	15372.32 ± 316.07 (2.056)	9.2
P10	<i>Populus euro-america</i>	18791.20 ± 248.45 (1.322)	16130.08 ± 229.78 (1.424)	7.5
P11	<i>Acer pseudoplatanus</i>	18637.91 ± 152.15 (0.816)	15615.05 ± 137.43 (0.880)	9.7
P13	<i>Chlorophora excelsa</i>	20314.74 ± 378.88 (1.865)	17287.67 ± 345.38 (1.998)	8.8
P14	<i>Entandrophragma cyli</i>	19053.87 ± 113.65 (0.596)	15691.61 ± 100.73 (0.642)	11.4
P15	<i>Gossweilerodendron b.</i>	20499.80 ± 338.74 (1.652)	17170.12 ± 303.73 (1.769)	10.3
P16	<i>Bowdichia nitida</i>	20809.47 ± 354.05 (1.701)	17907.85 ± 325.83 (1.819)	8.0
P17	<i>Hymenaea courbaril</i>	19296.38 ± 187.61 (0.972)	16183.69 ± 169.18 (1.045)	9.8

**Figure 2.1 Energy content for various biomass sources (6)**

In order to run the system continuously for 24 hours approximately 10 kg of eucalyptus globulus would need to be harvested. In order to keep the moisture content of the biomass down, the storage canister can be equipped with system to capable of removing and maintaining moisture levels.

### 2.2.5 Battery comparisons

There are numerous types of batteries and battery technologies available to choose from. In order to select appropriate energy storage device a comparison, on the characteristics of these various batteries, is done.

<i>Battery Type</i>	<i>Chemistry</i>	<i>Specific energy (Wh/kg)</i>	<i>Specific energy (J/kg)</i>	<i>Energy density (Wh/L)</i>	<i>Cost (\$/Wh)</i>
Alkaline	Alkaline	110	400,000	320	0.19
Lithium-ion	Li-Ion	128	460,000	230	0.47
Carbon-zinc	C-Zn	36	130,000	92	0.31
Lithium thionyl chloride	Li-SOCl <sub>2</sub>	700	2,000,000	1100	1.16
Lead acid	Pb acid	41	146,000	100	0.17
Nickel metal hydride	Ni-MH	95	340,000	300	0.99

**Table 2.3 Comparison of various batteries (7)**

The most common rechargeable batteries were investigated in the table above. In the interest of both cost and weight the lead acid battery is chosen. This chemistry is both cheaper and lighter than the remainder while also being able to satisfy the energy requirements of this task. Moving forward on this system in the future, alternate storage devices with higher energy densities could be used when the need arises.



## Chapter 3: Sensory system

### 3.1 Introduction

The sensory system is a combination of various sensors/controllers which work together to provide and execute information for the EATR system. Based on their characteristics, each is assigned a specific task. This chapter investigates the physics of the various components used in system. The functional decomposition of the system is illustrated below.

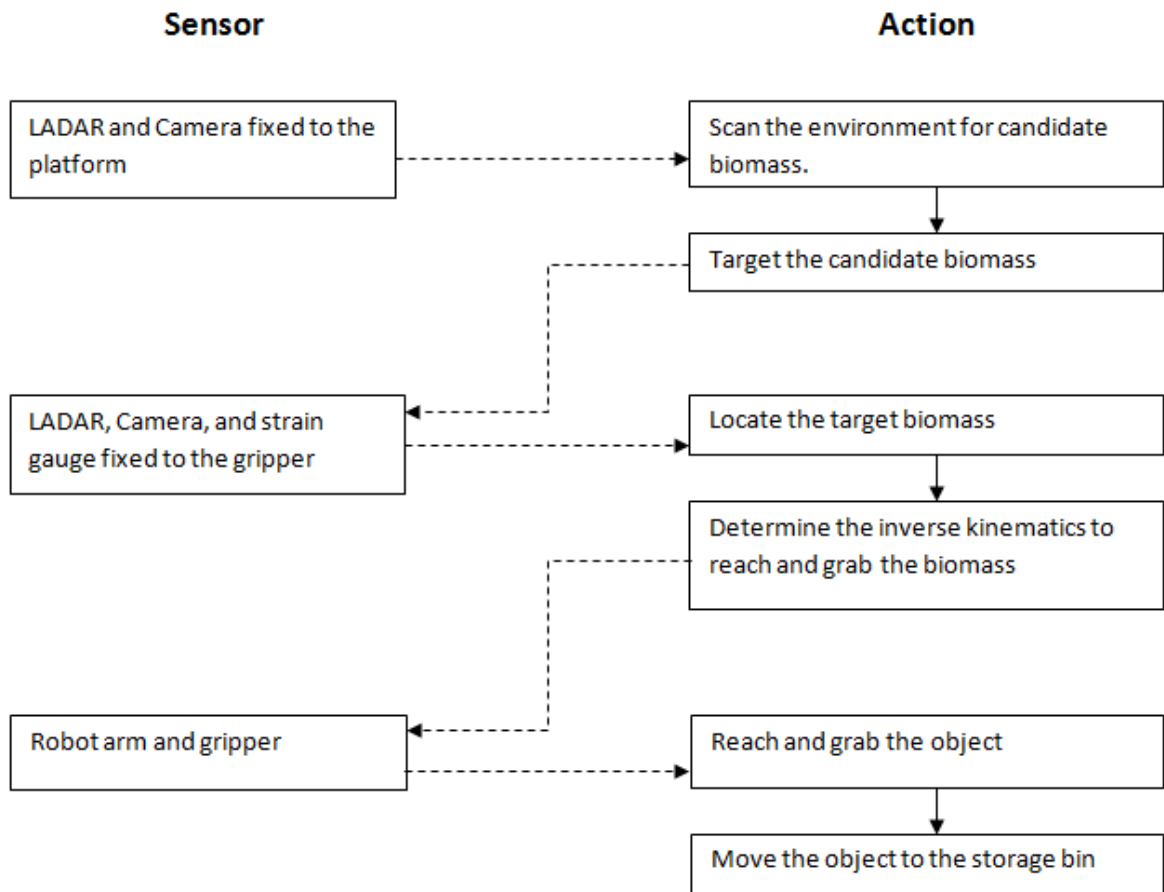
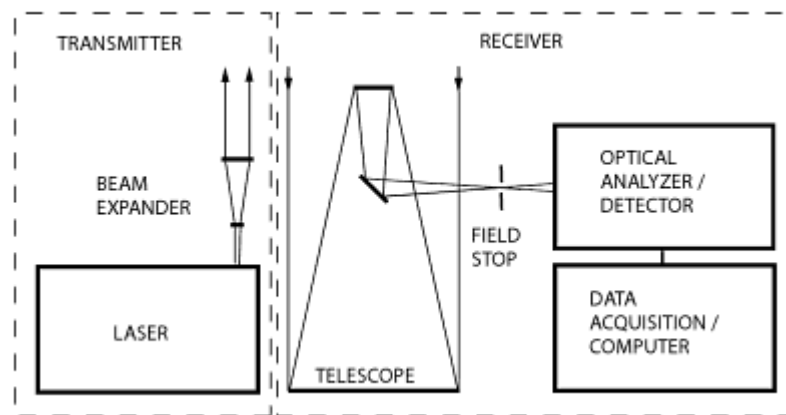


Figure 3.1 Sensory system criteria

### 3.2 Components

#### 3.2.1 Ladar

The LADAR (laser detection and ranging) system is a device capable of scanning and mapping out a 3D area. Similar to RADAR, the LADAR emits an electromagnetic signal, photons, that are reflected back after coinciding with a target. The received photons are then converted into a charge by the means of a photodiode. This charge, proportional to the incoming photons, is then sent to be analyzed by the acquisition system.



**Figure 3.2 Ladar system (8)**

Electromagnetic energy travels at the speed of light, hence the relationship between the range and the travel time is given by:

$$t = \frac{2R}{c}$$

**3.1**

$c$  is the speed of light in air. Solving for the range yields:

$$R = \frac{ct}{2} = t_{ns}(.150m)$$

**3.2**

The LADAR equation is the link between the power of the detected incoming photons and the physical parameters of the environment and LADAR setup. The most general form of the equation is written as (8):

$$P(R) = KG(R)\beta(R)T(R)$$

3.3

The incoming power  $P$  is a function of the distance  $R$  and is composed of four factors.  $K$ , the system factor, and  $G(R)$ , the measurement geometry, are specific to LADAR setup. On the other hand,  $\beta(R)$ , the backscatter coefficient and  $T(R)$ , the transmission term, are environment specific and thus need to be investigated.

The system factor,  $K$ , can be written as

$$K = P_0 \frac{c\tau}{2} A\eta$$

3.4

$P_0$  is the average power emitted by a single laser pulse and  $\tau$  is the temporal pulse length.  $A$  is the backscattered light receiving area of the Ladar and  $\eta$  represents the total efficiency of the LADAR system (8).

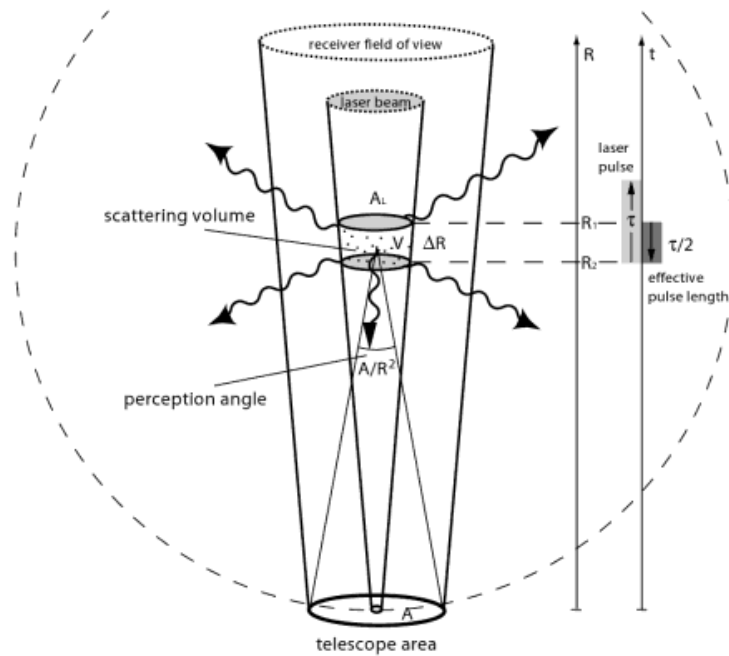


Figure 3.3 Photons in the LADAR path (8)

The geometric factor,  $G(R)$  is written as

$$G(R) = \frac{O(R)}{R^2}$$

3.5

$O(R)$  is the laser-beam receiver-field-of-view overlap function. This results from the combination of all the geometric effects. At the LADAR the value is zero and becomes unity as the beam is completely imaged onto the detector. The  $R^{-2}$  is the dominant factor responsible for the LADAR's large dynamic range. This is due to the fact that the LADAR's receiving area coincides with the surface of the sphere that the backscattered light lies in (8).

The backscatter coefficient,  $\beta(R, \lambda)$ , corresponds to the amount of light being received by the LADAR back from the atmosphere. It is the dominant atmospheric factor in

determining the strength of the returning signal. Accounting for all kinds of scatters, it is written as

$$\beta(R, \lambda) = \sum_j N_j(R) \frac{d\sigma_{j,sca}}{d\Omega}(\pi, \lambda)$$

3.4

Here,  $N_j$  stands for the concentration of  $j$  scattering particles within the illuminated sphere. The particles backward differential scattering cross section is represented by  $d\sigma_{j,sca}(\pi, \lambda)/d\Omega$ . In most environments, the backscattered is due to its interaction with air molecules and particulate matter. Hence the backscatter coefficient is the sum of both these contributions (8).

$$\beta(R, \lambda) = \beta_{mol}(R, \lambda) + \beta_{aer}(R, \lambda)$$

3.5

The transmission term,  $T(R, \lambda)$  accounts for the fraction of light which is lost from the initial laser pulse and is given as

$$T(R, \lambda) = \exp\left[-2 \int_0^R \alpha(r, \lambda) dr\right]$$

3.6

The light extinction coefficient,  $\alpha(R, \lambda)$ , is the sum of all transmission losses and is integrated over the distance the light travels in both its outgoing and return path. It can be written as

$$\alpha(R, \lambda) = \sum_j N_j(R) \sigma_{j,ext}(\lambda)$$

3.7

Similar to the backscatter coefficient, it is defined as the product of the concentration of particles and  $N$ , and extinction cross section,  $\sigma_{ext}$  of a scatter particle  $j$ . Due to the

fact that light can be lost to both scattering and absorption by particles, the extinction coefficient is written as the sum of the contributions (8).

$$\alpha(R, \lambda) = \alpha_{mol,sca}(R, \lambda) + \alpha_{mol,abs}(R, \lambda) + \alpha_{aer,sca}(R, \lambda) + \alpha_{aer,abs}(R, \lambda)$$

**3.8**

Similarly, the extinction cross section is also due to both scattering and absorption.

$$\sigma_{ext}(\lambda) = \sigma_{sca}(\lambda) + \sigma_{abs}(\lambda)$$

**3.9**

Therefore the LADAR equation can be written as (8).

$$P(R, \lambda) = P_0 \frac{c\tau}{2} A_\eta \frac{O(R)}{R^2} \beta(R, \lambda) \exp \left[ -2 \int_0^R \alpha(r, \lambda) dr \right]$$

**3.10**

This equation governs the fundamental operations of a LADAR. Variations of this equation are used in different LADAR setups depending on the environment and requirements of the experiment. Background noise is also a significant contribution to the error and varies based on the environment. It is accounted for by subtracting a data sample free of any laser-backscattered photons.

### 3.2.2 Video Camera

A video camera is a device capable of capturing a series of digital images and storing them for later acquisition. A digital image is a representation of a real world scene composed of discrete elements called pixels. Images are composed of a matrix of square pixels arranged in columns and rows. In general pixels are characterized by two main parameters, position and intensity. The position of a pixel refers to its row and column location in the matrix it lies in. The intensity of a pixel describes the

color output that it will be displaying. A “true color” image is has a 24 bit color depth composed of three 8 bit color depths, red, green, and blue. Every pixel in this matrix has assigned intensities, one for each of the three colors, ranging between 0 and 255. Combinations of these three colors form a broad array of colors (9).

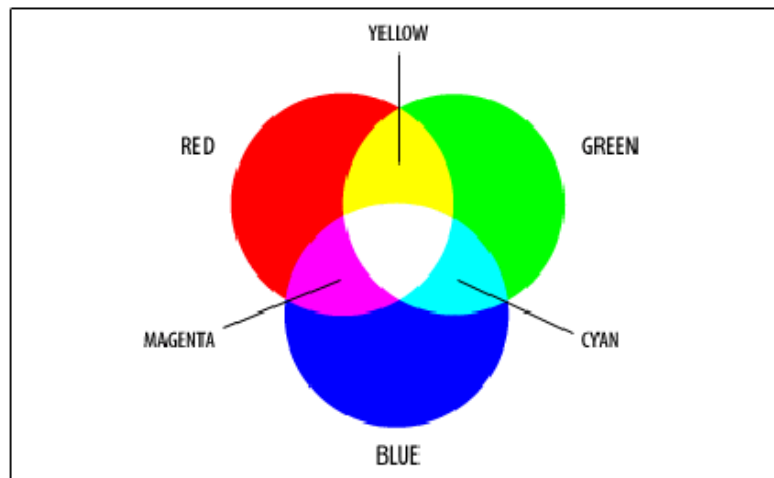


**Figure 3.4 The additive model of RGB. Red, green and blue are the primary stimuli for the human color perception and are the primary additive colors (9).**

Object detection is the task of extracting an object of interest from an image by differentiating certain features of interest. To distinguish between various objects in an image, a process called segmentation is employed. Image segmentation is the process of dividing an image in to various meaningful segments based on a given application. This division is done by grouping pixels with similar characteristics together according to properties such as color, intensity or texture. Image segmentation is done using various types of edge detection techniques.

Edge detection analysis is done by segmenting the image based on abrupt discontinuities between pixels. These sharp changes in intensity characterize the boundaries of objects. The three main steps in edge detection are filtering, enhancement, and detection (10).

*Filtering* is necessary in order to improve the effectiveness of the edge detector with respect to noise.

*Enhancement* is the process of then emphasizing the pixels where the abrupt changes in intensity occur.

*Detection* occurs by assigning a “0” value for any pixel outside of the given threshold and a “1” for any that lie within the threshold. This creates a binary black and white image with the edges outlined in black.

The majority of different edge detection techniques may be grouped into two categories, gradient based or laplacian based. Gradient based techniques find edges by looking for the maxima and minima of the first derivative whereas the laplacian method searches for the zero points in the second derivative.

### 3.2.3 Robot Arm

The robotic arm is the device capable of reaching and grabbing candidate biomass and dispensing them in the given location. The arm being used is constructed by Elbit Systems of America, has a 48” reach with 6 degrees of freedom (DOF). Once a candidate biomass is identified, it is up to the arm to locate, grab and store the object. This is achieved by calculating the required forward and reverse kinematics.



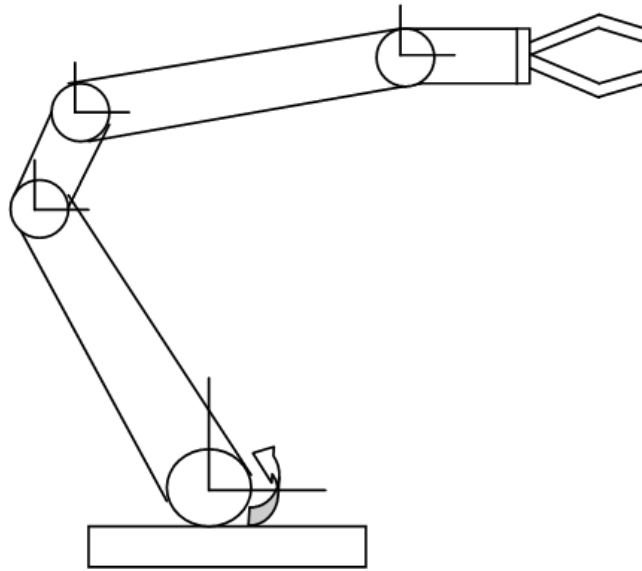


**Figure 3.5 Robot arm with degrees of freedom**

At rest the rest all the components of the arm sit at  $(x=0, y=0, z=0, \theta=0, \varphi=0)$ . The video camera and ladar are used to scan and locate potential biomass. After processing the image and determining the location of the object, the coordinated are sent to the arm which calculates the kinematics needed for it to reach and grab the object. Once grabbed, the arm will then proceed to drop the object at the canisters preset coordinates before returning to rest.

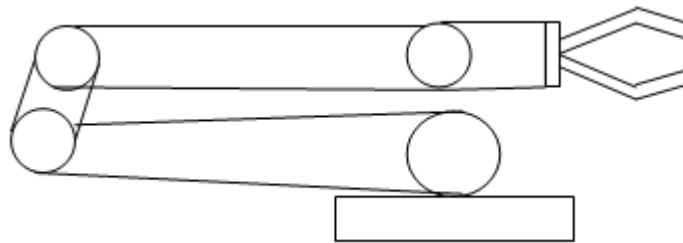


**Figure 3.6 The robot arm at rest**

In order to confirm the object has been gripped, a strain gauge is placed at the grippers end. Once the object is gripped an increase in strain is measured. The strain

gauge is a variable resistor supported by an insulated flexible backing. The resistor is connected to a wheatstone bridge circuit to measure the change in resistance.

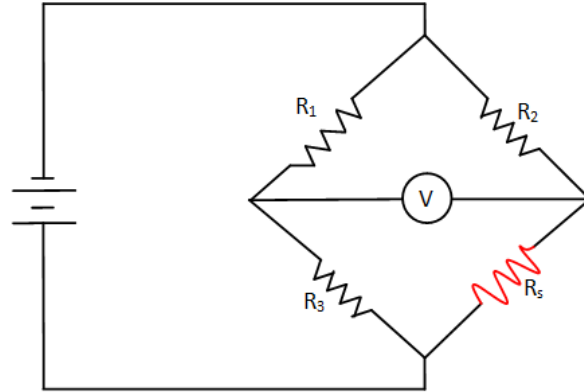


**Figure 3.7 Wheatstone bridge**

By setting  $R_1 = R_3$  and  $R_2 = R_s$ , with no strain on the strain gauge  $R_s$ , the voltage between the bridge will be zero. Compression in the gauge will cause the resistance to decrease and a tension in the gauge will cause the resistance to increase. This change in resistance will lead to a change in the voltage thus indicating a strain. The strain gauge can also be used to measure the mass of an object. Knowing the mass of an object will aid in determining the density, a useful material property.

Strain gauges are supplied with a gauge factor from the manufacturer. The gauge factor is a relation of the strain to the resistance change in the strain gauge and is given by (11):

$$GF = \frac{\Delta R / R_G}{\epsilon}$$

**3.11**

GF is the gauge factor,  $\Delta R$  is the change in resistance due to strain,  $R_G$  is the resistance in the undeformed gauge, and  $\epsilon$  is the strain. Hence the strain can be written as:

$$\varepsilon = \frac{\Delta R/R_G}{GF}$$

**3.12**

From hooks law:

$$\sigma = E_m \varepsilon$$

**3.13**

Where  $\sigma$  is the applied stress and  $E_m$  is the modulus of elasticity, or young's modulus, of the material the strain gauge is mounted on.

The applied stress can be calculated using:

$$\sigma = \frac{F}{A_c}$$

**3.14**

Where  $F$  is the applied force and  $A_c$  is the cross sectional area of the surface the gauge is mounted on. To calculate the mass of the object equation can be rewritten as:

$$F = ma$$

**3.15**

$$\sigma = \frac{ma}{A_c}$$

**3.16**

$$\frac{ma}{A_c} = E_m \varepsilon$$

**3.17**

Where  $m$  is the mass of the object and  $a$  is the acceleration due to gravity,  $9.8 \text{ m/s}^2$ .

Hence the mass of the object is found from the strain gauge using:

$$m = \frac{\Delta R/R_G A_c E_m}{GF a}$$

### 3.2.4 Relative humidity (RH) sensor

A RH sensor is a device capable of measuring the amount of water vapor in an air/water vapor mixture. In an analog RH sensor, a capacitor based system is used to gauge the amount relative humidity. Generally the film capacitor is composed of either glass or ceramics. Accompanied is an insulating polymer material which absorbs and releases water based on the relative humidity of the air. This absorption causes an expansion which in turn changes the capacitance of the film thus changing the voltage (12).

$$C = \frac{q}{V}$$

3.19

$C$  is the capacitance,  $q$  is the charge and  $V$  is the voltage.

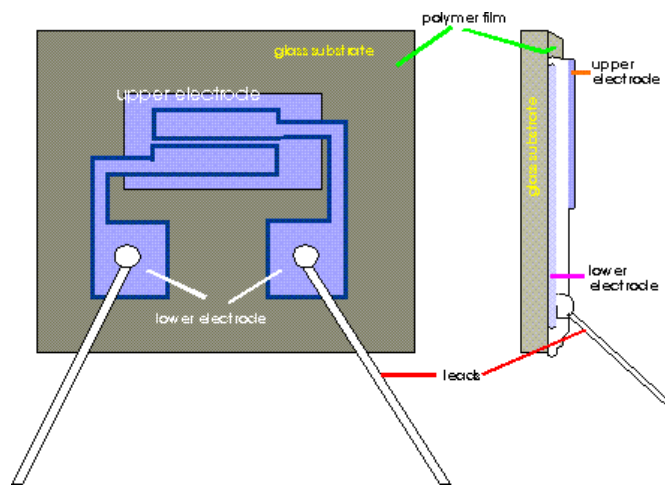


**Figure 3.8 Schematic of an RH sensor (13)**

The output signal of the sensor will depend on, and is proportional to, the input signal. The output voltage is equivalent to a factor of the percent relative humidity and the input voltage (12).

$$V_{out} = \%RH(V_{in})$$

3.20

$$\%RH = \frac{V_{out}}{V_{in}}$$

### 3.2.5 Oxygen sensor

The oxygen ( $O_2$ ) sensor is used to monitor the ratio of the air and fuel mixture of the exhaust gasses. The sensor is composed of a zirconium ceramic bulb which is coated with a porous layer of platinum on the outside and two strips of platinum on the inside, acting as electrodes. The outside of the sensor is heated by the exhaust gasses flowing across it. On the other hand, the inside of the sensor is by the outside air which flows into the sensor via the wire gaps running through the middle. Voltage flows through the ceramic bulb based on the difference in oxygen levels between the exhaust gasses and the outside air (14).

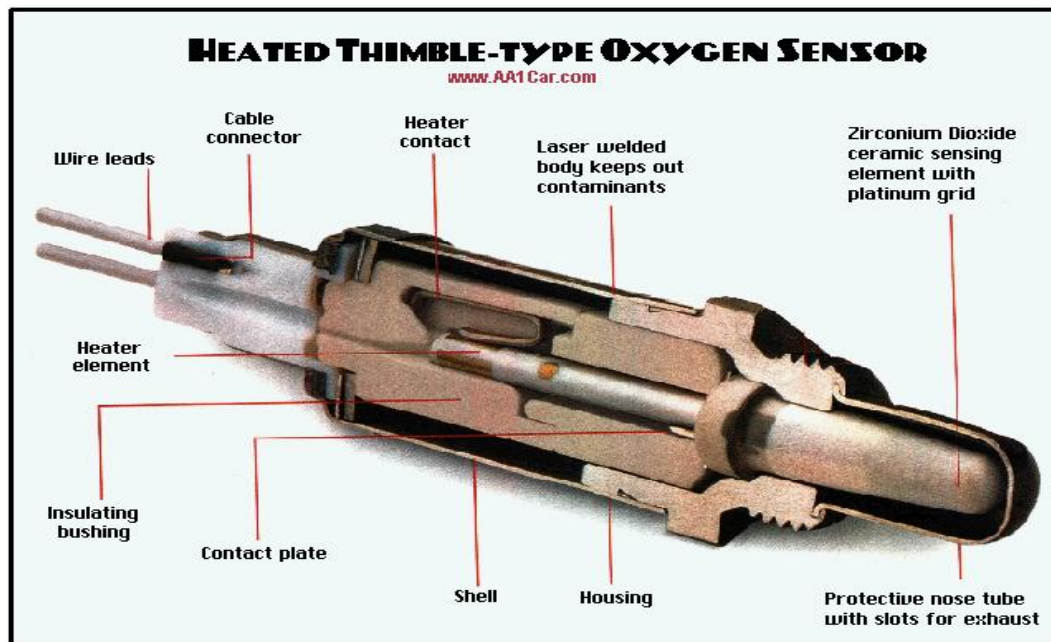


Figure 3.9 Diagram of an  $O_2$  sensor (14)

Typically a narrow band O<sub>2</sub> sensor will generate up to 0.9V for a rich fuel mixture, 0.2V when the mixture is lean and 0.45V when the mixture is at equilibrium, approximately 14.7 to 1, for octane fuel. For wood however, a good combustion would be considered to be a ratio of 10-12 pounds of wood to 1 pound of air (15). Hence an output of 0.8V-1V indicates a mixture at equilibrium. Voltages below 0.8 would indicate a lean mixture and voltages above 1 would mean a rich one.

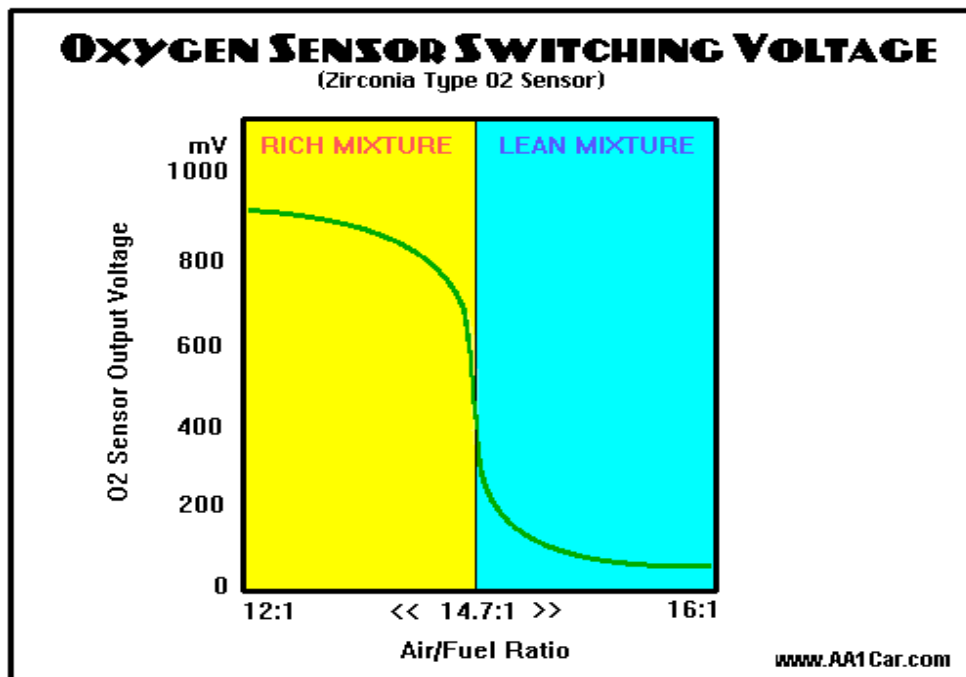


Figure 3.10  $V_{out}$  vs air/fuel ratio for an O<sub>2</sub> sensor (14)

### 3.2.6 Arduino UNO

The Arduino is simple, open source electronic prototyping platform. It is designed to be able to use a variety of both analog and digital inputs to control a slew of sensors. The platform uses the Arduino programming language and can operate both stand alone or collaborating with a computer. The heart of the Arduino is the ATmega328 microcontroller. The ATmega328 is an 8-bit AVR RISC-based microcontroller which combines 32KB ISP flash memory with read-while-write capabilities, 1024B

EEPROM, 2KB SRAM, 23 general purpose I/O lines, 32 general purpose working registers, three flexible timer/counters with compare modes, internal and external interrupts, serial programmable USART, a byte-oriented 2-wire serial interface, SPI serial port, a 6-channel 10-bit A/D converter (8-channels in TQFP and QFN/MLF packages), programmable watchdog timer with internal oscillator, and five software selectable power saving modes (15).



**Figure 3.11 Arduino board (15)**

## Chapter 4: Energy system

### 4.1 Introduction

The energy system includes a combination of components required to not only convert the biomass fuel to an electrical source, but also to store, monitor and regulate the energy. Each component is unique in its role on the system. This chapter investigates the components involved in the energy conversion process and their role in the system. The functional decomposition of the energy system is illustrated in the following flow chart.

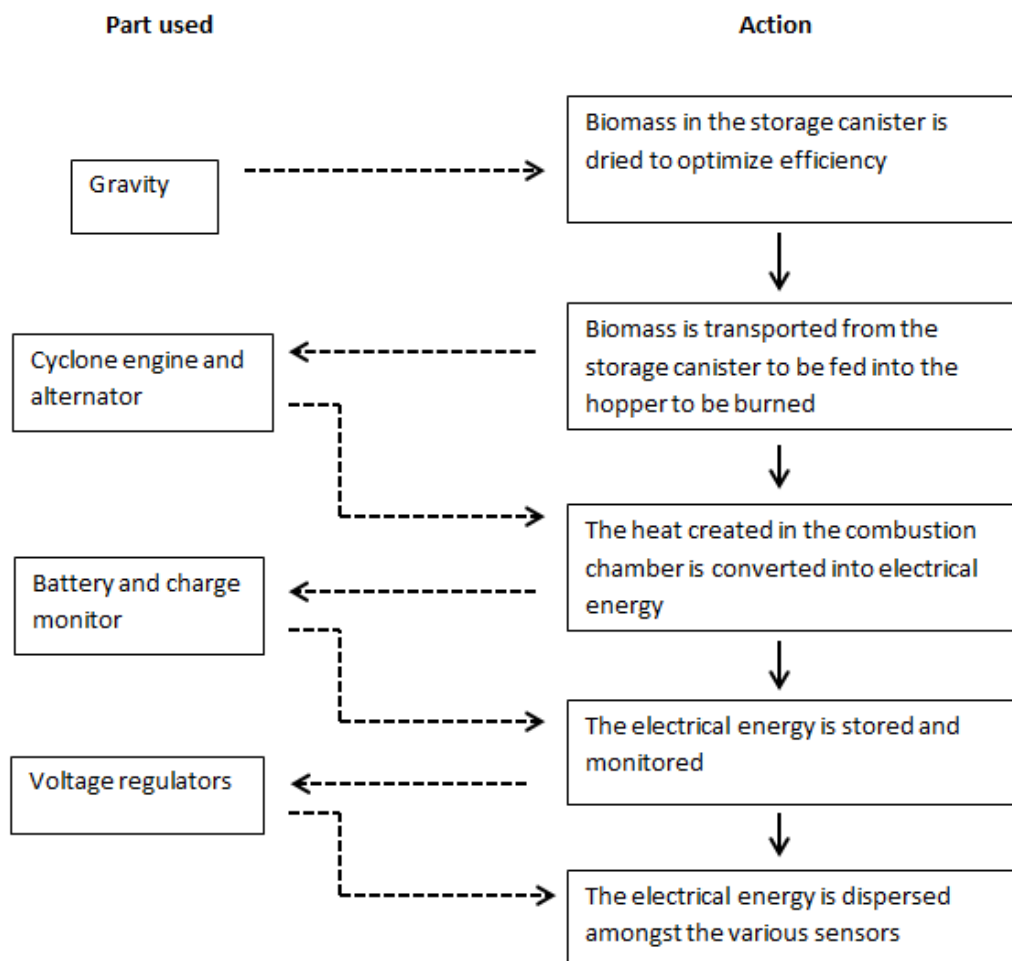


Figure 4.1 Energy system criteria



## 4.2 Cyclone engine components

In order to burn the biomass and convert the heat to electricity, an external combustion, Rankine cycle heat regenerative external combustion engine is used. In short, this is a high efficiency compact steam engine. The engine was designed and manufactured by Cyclone Power Technologies however additional circuitry is needed to integrate the system. To initially power up the engine an external pair of 12v, U1 style batteries in series is needed. In order to adequately distribute power to the various components a power converter circuit must be designed.

### 4.2.1 Hopper and feeder

The hopper is an enclosed dry storage area used to hold retrieved biomass. It is equipped with a safety fire extinguishing system that engages when the hopper temperature exceeds 180°F. The system discharges a gas that displaces the oxygen in the volume halting the production of fire. The biomass is fed from the hopper to the burner, as determined by the charging system, through a helix shaped feeder (16).

### 4.2.2 Burner

The burner is manufactured and controlled by an off the shelf product from pellx. The pellx controller allows for the adjustment of startup features for the burner. These adjustments need be changed based on the fuel source characteristics. Some of the variable features are: the size of the initial starting feed, the feed rate of pellets, and the fan speed. Since the pellx controller is adjusted manually and the EATR requires

autonomous control an integrated controller must be designed to automatically adjust the burner for the change in the incoming biomass (16).

#### 4.2.3 Heat exchanger

The heat exchanger is composed of a series of insulated stainless steel coils atop of the burner assembly. Water in the tubes is maintained at a pressure between 200 and 600 PSI, during normal operation, by an engine driven high pressure pump. A smaller 12v 125PSI pump drives water from a filtered reservoir to the high pressure pump. This smaller pump also acts as a startup pump when the engine is shutoff and the high pressure pump is not on (16).

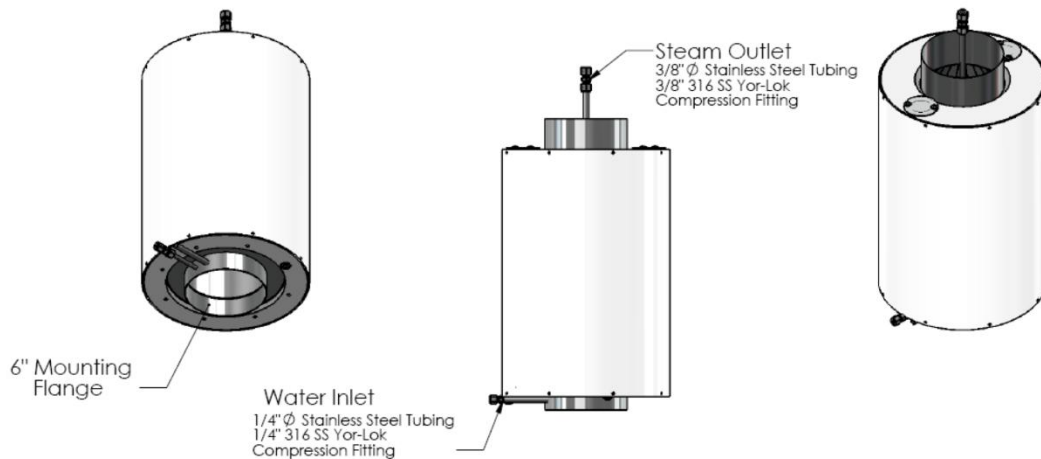


**Figure 4.2 Heat exchanger of the cyclone engine (16)**

#### 4.2.4 Waste heat engine

The waste heat engine is a radial configured 6 cylinder rankine cycle external combustion engine. The engine is both lubricated and condensed by running water. A 45psi, 12v pump pushes water into the top of the engine lubricating and condensing the steam exiting the pistons then returning to the radiator (16).

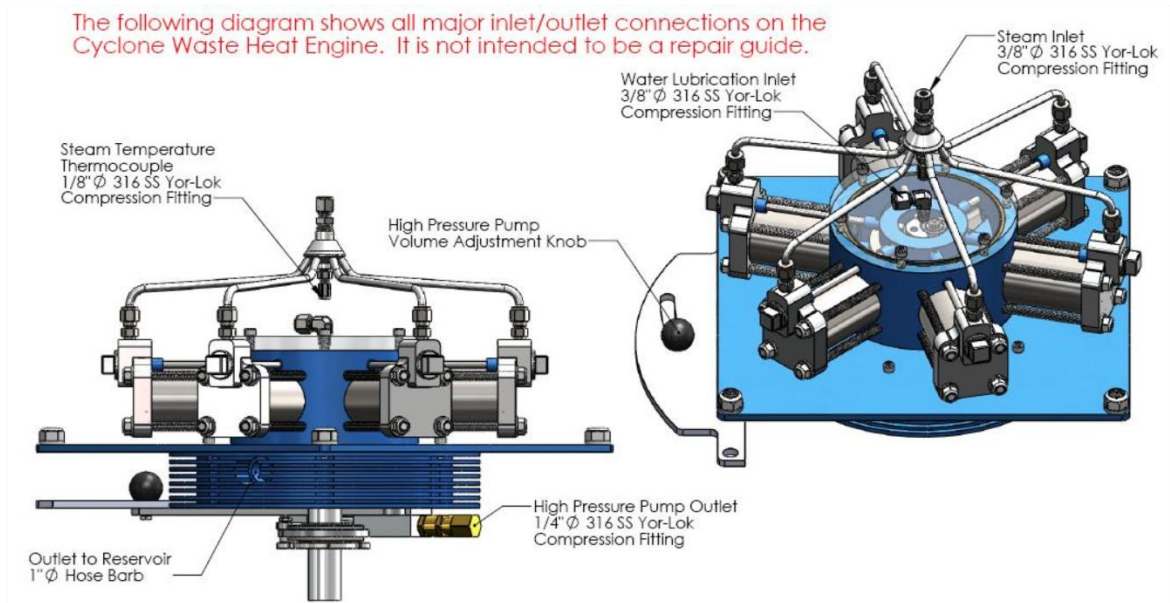


**Figure 4.3 Major inlet and outlet connections for cyclone waste heat engine (16).**

#### 4.2.5 Condenser system

The condensation system on the engine is composed of a cool water inlet on the top of the engine, a finned pan with an enclosed impeller under the engine, a radiator with powerful cooling fans, and a reservoir with a very fine micron filter. Cool water, for lubrication and condensation is circulated from the bottom to the top by a 45 psi, 12v, water pump. In order to keep the pump primed, it is necessary to keep the de-mineralized water level in the 7 gallon reservoir at the top (16).

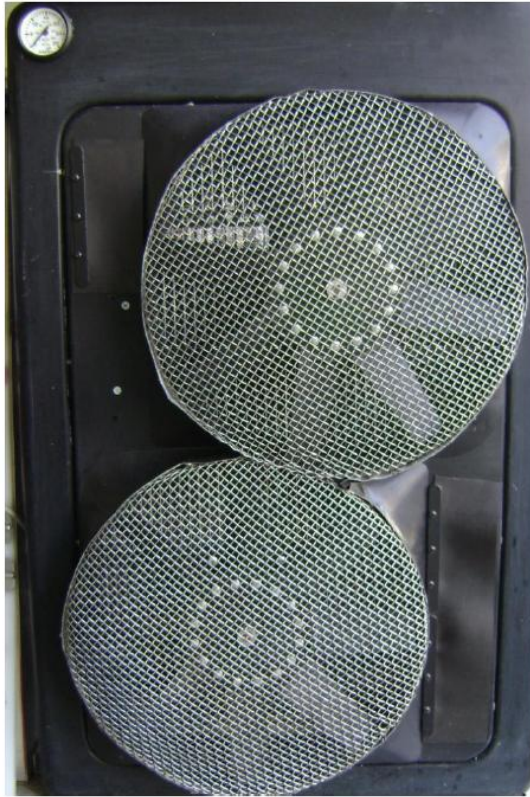


**Figure 4.4 Condenser fans (16)**

#### 4.2.6 Alternator

Steam from the power generator is converted into electrical energy using a 24v DC alternator. The maximum output current is 174 Amps with an engine to alternator pulley ratio of 3.2:1. The onboard battery of the engine is used to power the essential components of the engine such as the pumps, fans, burner, etc. For this reason an external battery post is set up to be charged by the engine and supply power to the various EATR components. There is an inverse relationship between the alternator output and charge state of the batteries. Therefore the alternator will output its maximum charge, based on the RPM, when the batteries become low.

The alternator was tested for 30 hours yielding an output of approximately 1.7 kilowatts of power at 666 engine RPM and over 2.0 kilowatts at 946 engine RPM (16).

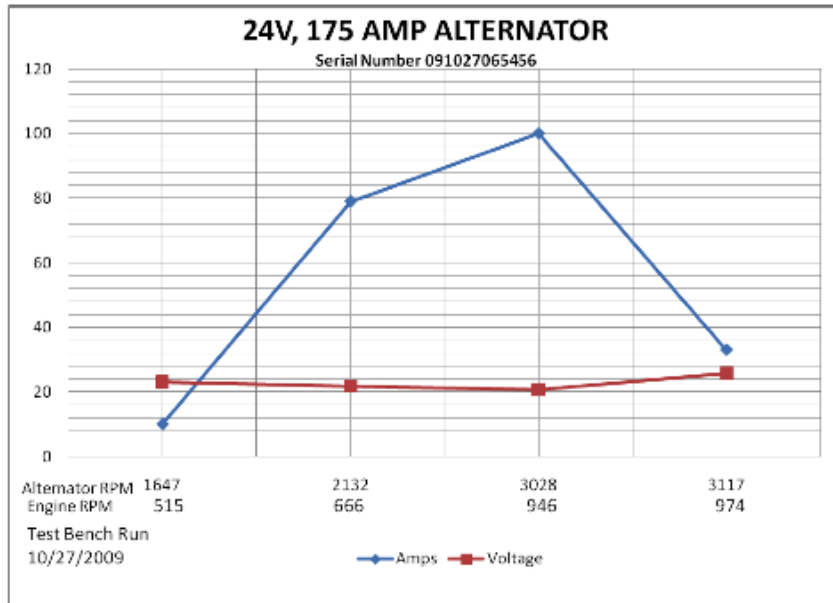


Figure 4.5 Alternator output (16)

4.2.7 Engine illustration and setup

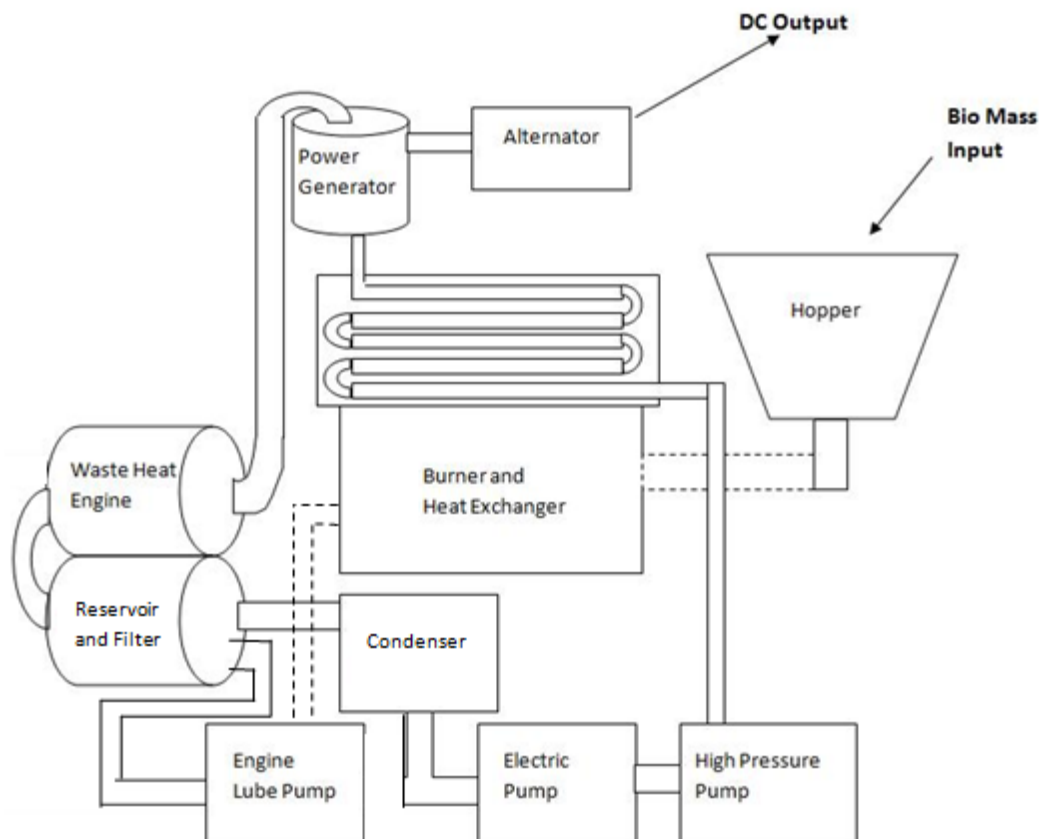


Figure 4.6 Schematic of cyclone engine

### 4.3 Wood chipper

In order for the collected wood/biomass to be burned in the engine, a wood chipper must be used to shred the wood to a size able to fit in the hopper. The chipper should be able to accommodate various types and sizes that would be found in its environment. Based on the geometry and setup of the engine, no commercial wood chipper that could be easily be integrated currently exists. For this reason one must be designed for this specific setup. The chipper would have to be placed above the hopper. An investigation into the potential design of the chipper is done.

The main components of a wood chipper are:

- The motor and pulley assembly used to supply and transfer power to the chipping unit.
- The cutting unit which chops the wood into smaller pellets.

At this time, the chipper would only be required to process smaller pieces of fuel, such as tree shrubs, so a large, powerful motor is not needed. The first step in designing the chipper is to estimate the power of the motor need to spin the cutting unit. The following assumptions are made:

- The weight of the cutting blades is  $\sim 2.5\text{kg}$ .
- The length of the blades is  $\sim 0.5\text{m}$ .
- The only resistive force on the cutting bladed is the weight of the wood in the chipper hopper  $\sim 17\text{kg}$ .
- The efficiency of the motor is 25%.
- The motor will achieve maximum horsepower at 2000 RPM's.

The torque required to spin the blades is a product of the force and the distance.

$$T = Fd$$

4.1

$$T = \left[ (2.5kg) \left( 9.8 \frac{m}{s^2} \right) + (17kg) \left( 9.8 \frac{m}{s^2} \right) \right] (0.5m)$$

$$T = 95.55Nm = 70.77ft \cdot lbs$$

The most common rating for the power of a motor is horsepower (*hp*).

$$hp = \frac{T(RPM)}{5252}$$

4.2

$$hp = \frac{70.77ft \cdot lbs(2000)}{5252} = 26.95hp$$

$$26.95(.25) = 6.73hp$$

In order to compare our results with commercially available wood chippers a plot of various wood chipper horse power (*hp*) is plotted against the chipping capacity, the diameter of wood a unit will accept. A curve fit yields the equation used to approximate the hp required for a give chipping capacity. The following data was taken from a consistent commercial manufacturer (17).

Chipping Capacity ( <i>in</i> )	Power( <i>hp</i> )
3.5	4.38
4.5	6.28
5.5	11.42
6.5	20.94

**Table 4.1 Chipping capacity vs. power required**

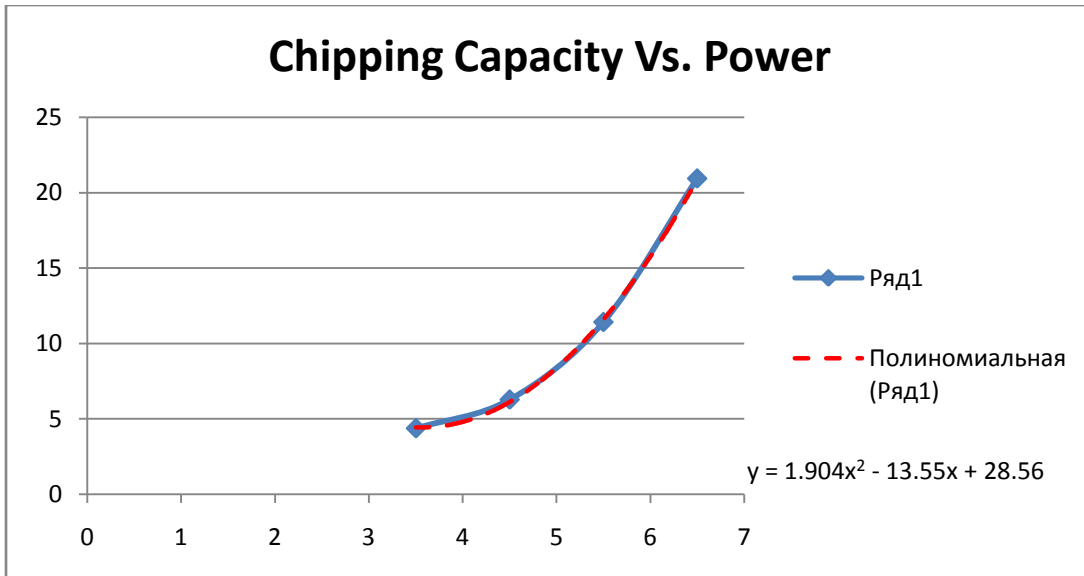


Figure 4.7 Plot of chipping capacity vs. power required

The radius of 17kg log of wood can be approximated using the volume of a cylinder and the density of wood. Assuming the average density ( $\rho$ ) of a 2ft piece wood equal to  $600\text{kg}/\text{m}^3$  the volume is found using:

$$\rho = \frac{m}{V} \Rightarrow V = \frac{m}{\rho}$$

4.3

$$V = \frac{17}{600} 0.0283\text{m}^3$$

$$V_{cylinder} = \pi r^2 h$$

4.4

$$r = \sqrt{\left(\frac{V_{cyl}}{\pi h}\right)} = \sqrt{\frac{(0.0283\text{m}^3)}{\pi(0.61\text{m})}} = 0.05916\text{m} = 2.33\text{in}$$

It can be assumed that a 17kg piece of wood has a radius of approximately 2.33in.

From the equation fit for commercial wood chippers a 7.31hp engine would be needed to chip this piece of wood.



$$y = 1.904x^2 - 13.557x + 28.561$$

$$1.904(2.33)^2 - 13.557(2.33) + 28.561 = 7.3095hp$$

The power required, according to the commercial approximations is within 10% of the designed motor. The blades of the cutter are recommended to be of hardened steel in order to maximize the rigidity and allow for the chipping of tougher wood. The following figure shows the placement of the chipper with respect to the engine.

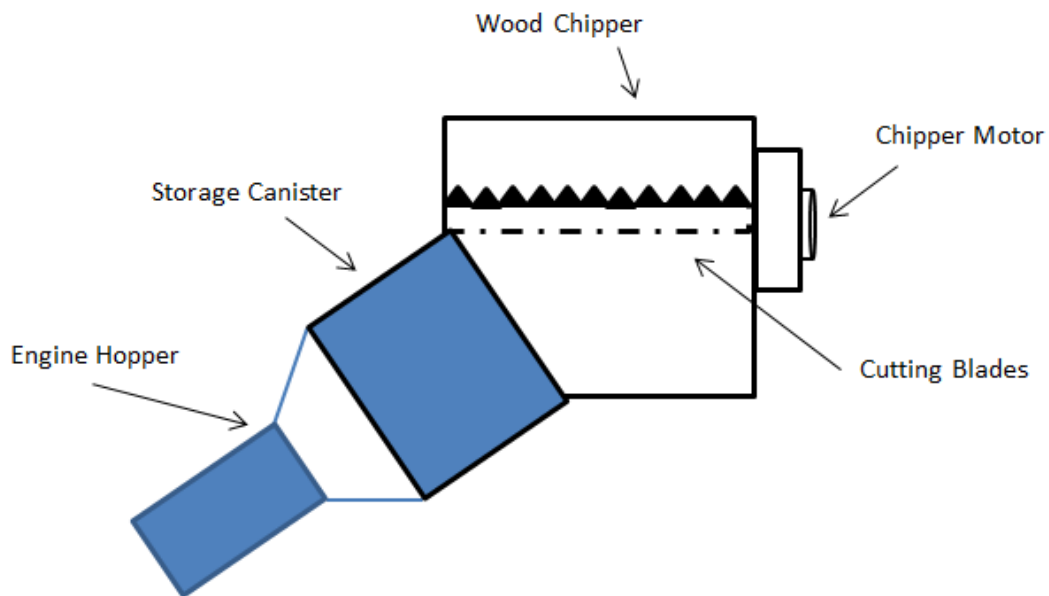


**Figure 4.8 Wood chipper design and placement**

#### 4.4 Battery Setup

In order to select the number and wiring of the batteries to be used, a minimum lifetime of the system without any charge must be assumed. For this case, 24 hours is assumed to be a sufficient operating time of the system. With a power requirement of 470 W and a 24 V output this yields a 470 AH capacity to be needed to power the system for 24 hours. This can be achieved using twenty Huamo HM12-50 batteries.

These are 12 V, 50AH batteries which can be wired in series to obtain the 24 V output needed (18). The BZ MPPT500HV charge controller is wired between the charging system and the batteries in order to protect the batteries from overcharging and provide a triggering signal to the engine to begin charging when they reach an unsafe voltage.

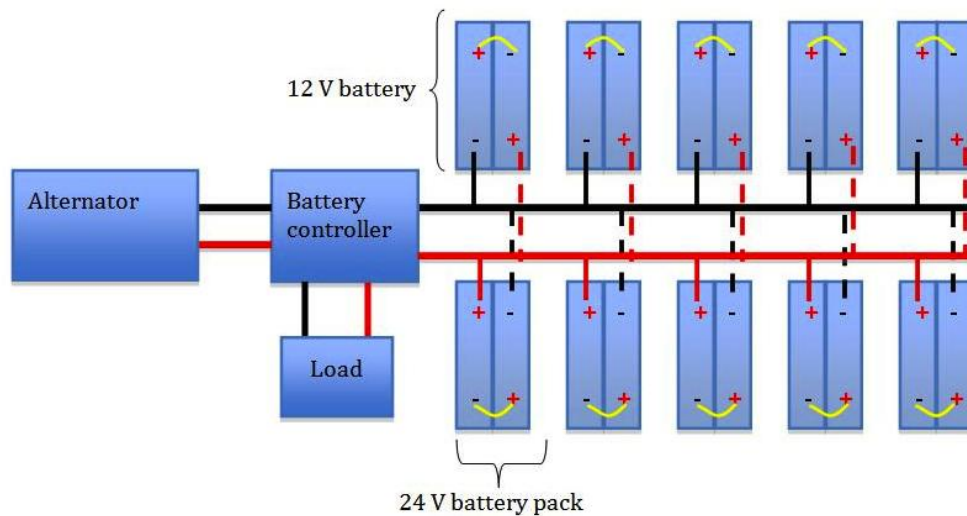


**Figure 4.9 Battery setup**

#### 4.5 Integration

In order to adequately provide power to all the smaller sub systems an LM2677 voltage regulator is used to step down the 24 V output of the battery. The LM2677 is an adjustable voltage regulator with an input voltage ranging between 8 V~ 40 V and an adjustable output voltage range of 1.2 V ~ 37 V with an output current of 5 A (19). The corresponding circuit is illustrated below.

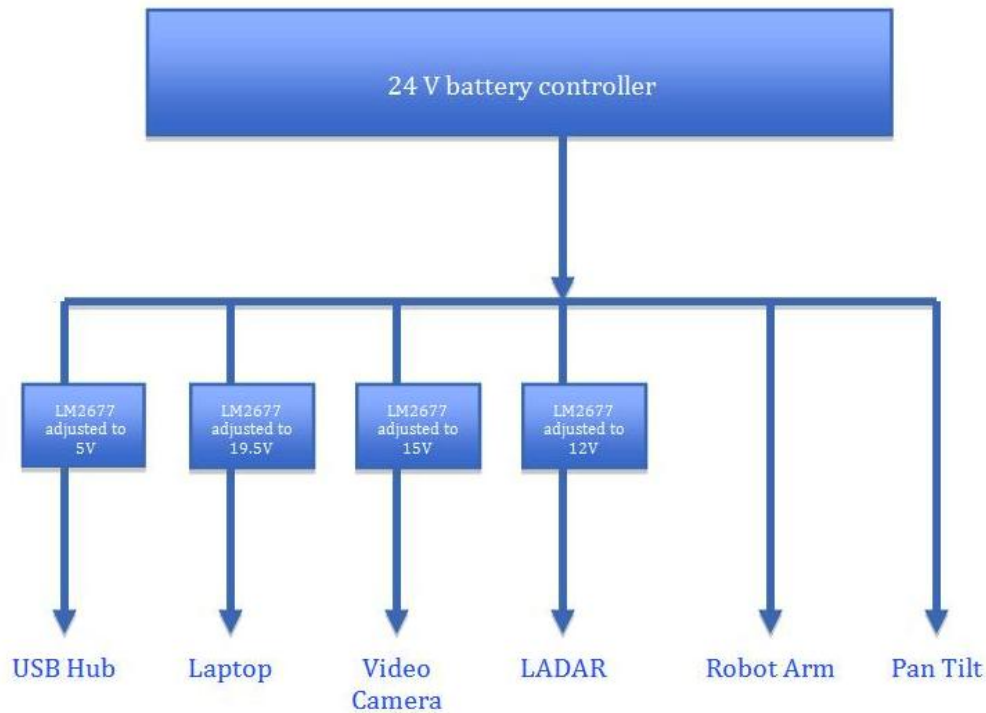


**Figure 4.10 Interface between battery outputs and sensors**

#### 4.6 Pellx controller

The pellx controller is used to calibrate the engine for optimal combustion of the biomass. Upon arrival, the engine was calibrated for a single wood pellet source. However, in a real world environment, multiple fuel sources exist creating the need for an integrated controller capable of achieving this optimization. The power switch in this case is bypassed, by the trigger wire from the battery monitor, due to the fact that the engine should only be running when a need to recharge the batteries occurs. The controller calibration process is as follows:

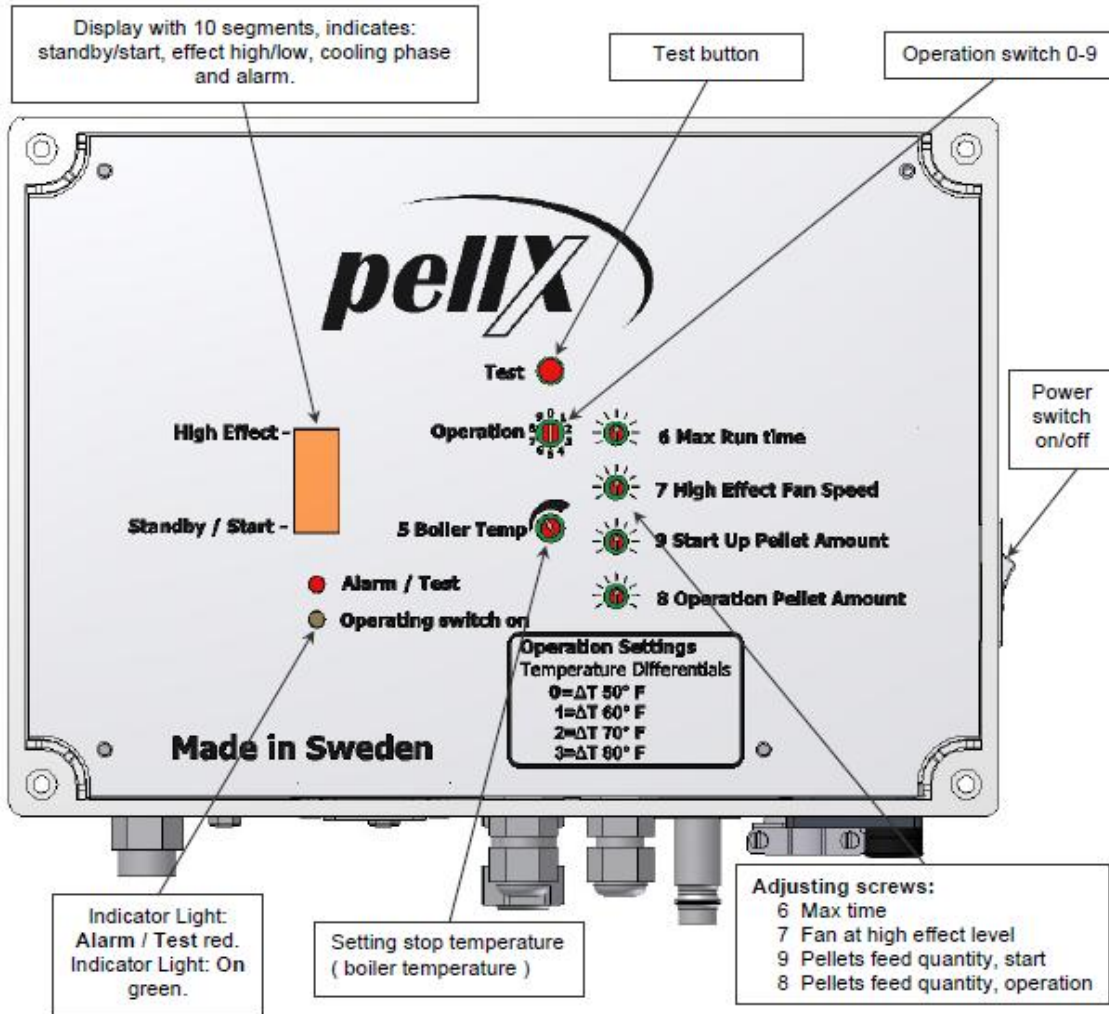


Figure 4.11 Pellx controller (20)

The run operation settings range from 0-9, allowing for numerous tests and adjustments. These operations need to be automated using a separate integrated controller (20).

*Run operation setting 0:* Sets the startup temperature to 50°F/10°C below the set maximum boiler temperature.

*Run operation setting 1:* Sets the startup temperature to 60°F/15°C below the set maximum boiler temperature.

*Run operation setting 2:* Sets the startup temperature to 70°F/20°C below the set maximum boiler temperature.

*Run operation setting 3:* Sets the startup temperature to 80°F/25°C below the set maximum boiler temperature.

*Test Function # 4: Function Test:* (Ignition element and fan run for 5 minutes. The flame sensor measures light intensity. (0 - 10 segments)) Turn the power switch to the off position. Turn the operation switch to # 4. Turn the power switch to the on position. The Test LED is off and the Operating LED flashes green. Push the test button once. The Test LED is on as solid red and the Operating LED flashes green. The heating element and fan run for 5 minutes. The flame sensor measures the light and displays the value on the LED bar.

*Test Function # 4: Self Cleaning Valve Test:* (Cycles the self-cleaning valves twice.) Turn the power switch to the off position. Turn the operation switch to # 4. Turn the power switch to the on position. The Test LED is off and the Operating LED flashes green. Push the test button once. The Test LED is on as solid red and the Operating LED flashes green. Wait 5 seconds or more. Push the test button twice. The Test

LED is off and the Operating LED flashes green. Both self-cleaning valves will open and close twice. Turn the burner off after the cycling of the valves.

*Test Function # 5:* Displays the boiler's turn off temperature and current temperature. Turn the power switch to the off position. Turn the operation switch to # 5. Turn the power switch to the on position. The Test LED is off and the Operating LED flashes green. Push the test button once. The Test LED is on as solid red and the Operating LED flashes green. The boiler's stop temperature (maximum temperature) is displayed by the number of green LED (2 - 10) bars. The stop temperature (maximum temperature) can be adjusted using the #5, Boiler Temp, potentiometer. Push the test button once. The boiler's current temperature is displayed by the number of green LED (2 - 10) bars. Push the test button once. The second temperature sensor (if installed) displays the current boiler temperature by the number of green LED (2 - 10) bars. Push the test button once. This cancels the test.

*Test Function # 6:* Maximum Run Time Adjustment. Turn the power switch to the off position. Turn the operation switch to # 6. Turn the power switch to the on position. The Test LED is off and the Operating LED flashes green. Push the test button once. The Test LED is on as solid red and the Operating LED flashes green. Push the test button once. The LED bars display the maximum run time with each LED bar equal to 30 minutes. The maximum run time can be adjusted using the #6, Max Run Time, potentiometer. If you have poor quality pellets and long run times, clinkers or sinter can form. Reducing the run time forces the burner to shut down and go through a

cleaning cycle. The burner will re-ignite and continue operation. Note that the maximum run time can be adjusted while the burner is in full operation mode without having to change the operation switch.

*Test Function # 7: High Effect Fan Speed.* Turn the power switch to the off position. Turn the operation switch to # 7. Turn the power switch to the on position. The Test LED is off and the Operating LED flashes green. Push the test button once. The Test LED is on as solid red and the Operating LED flashes green. The LED bar displays the maximum fan speed for high effect. The high effect fan speed can be adjusted using the #7, High Effect Fan Speed, potentiometer. When you adjust the #7 potentiometer, wait a couple of minutes and then recheck the flame quality and combustion gasses. Note that the high effect fan speed can be adjusted while the burner is in full operation mode without having to change the operation switch.

*Test Function # 8: Test and Adjust Pellet Feed Rate.* Turn the power switch to the off position. Turn the operation switch to # 8. Turn the power switch to the on position. The Test LED is off and the Operating LED flashes green. Push the test button once. (Note: When the test button is pressed once, the auger runs with 20 second pauses for 18 cycles. If the test button is pushed twice instead of once, the auger runs with only 2 second pauses for 18 cycles, reducing the total time of the test.) The Test LED is on as solid red and the Operating LED flashes green. The LED bar displays the feed rate and feeds pellets for 6 minutes. When you adjust the #8, Operation Pellet Amount, potentiometer, wait a couple of minutes and then recheck the flame quality and

combustion gasses. In #8 Test mode, collect the pellets during the 6 minute test, weigh them, and check the “supplied effect” graph in the installation manual (See section 5.1.3) to determine the BTU output. Note that the pellet feed rate “operation” can be adjusted while the burner is in full operation mode without having to change the operation switch.

*Test Function # 9: Start Up Pellet Amount.* Turn the power switch to the off position. Turn the operation switch to # 9. Turn the power switch to the on position. The Test LED is off and the Operating LED flashes green. Push the test button twice. The Test LED is on as solid red and the Operating LED flashes green. The LED bar displays the startup pellet amount. The startup pellet amount can be adjusted when you adjust the #9 Start Up Pellet Amount potentiometer. The startup amount of pellets should be around 1 cup / 200 - 250 grams / 7 - 8 oz. If the start amount is too low, the burner won't start. If the start amount is too high, the burner will “pop”. Note that the startup amount of pellets can be adjusted while the burner is in full operation mode without having to change the operation switch.

*Test Function # 9: To Load Pellet Auger: (Runs auger for 15 minutes.)* Turn the power switch to the off position. Turn the operation switch to # 9. Turn the power switch to the on position. The Test LED is off and the Operating LED flashes green. Push the test button once and wait 5 seconds. The Test LED is on as solid red and the Operating LED flashes green. Wait 5 seconds. Push the test button twice. The Test



LED flashes red and the Operating LED flashes green. The pellet auger runs for 15 minutes. The Test LED is off and the Operating LED flashes green.

The circuit schematic of the pellet controller is shown in the figure below. This schematic is used to incorporate the microcontroller allowing for active adjustment.

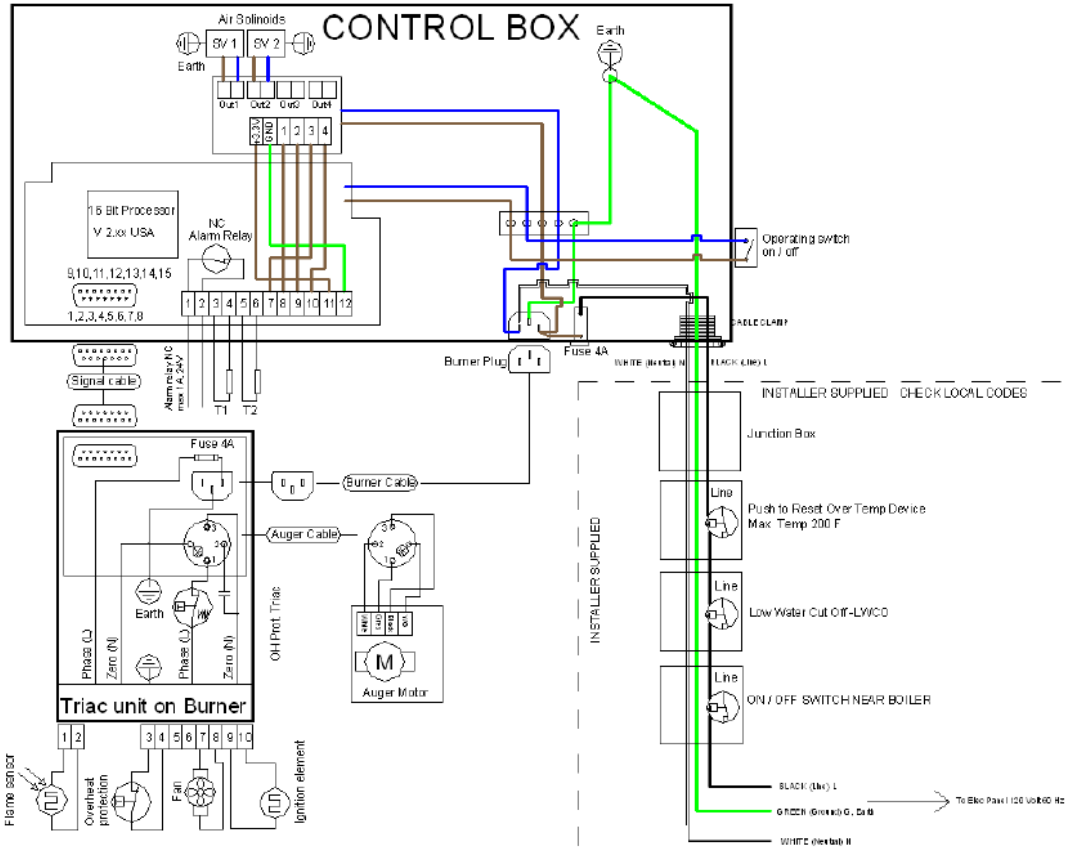


Figure 4.12 Schematic of the control box (16)

The boiler start, stop and differential temperature are assumed to remain constant in order to keep the alternator output the same. The size of the initial feed is also assumed to be the same due to the input geometry of the engine. Hence the remaining variables needed to be adjusted are the pellet feed rate, and the fan speed. For simplicity, the feed rate can remain constant as adjusting the fan speed alone would

accomplish an optimized combustion. In order to accurately adjust this setting, the flame quality and combustion gasses must be checked. This can be done using a narrow band O<sub>2</sub> sensor.

## **Chapter 5: System Integration**

### 5.1 Introduction

After evaluating the individual components, the system integration was carried out. The major components of the sensory systems are first mounted and connected followed by the energy system and integration of the control system. In this chapter the integration process of the various systems is detailed.

### 5.2 Sensory system integration

#### 5.2.1 Mounting the system components

The webcam and LADAR are mounted together onto the robotic arm from the same reference point. This allows for ease of calculating the distance to an object and referencing it back to the image. The webcam is adhered to the back of the LADAR using double sided tape. This allows for a simple yet secure mount. The LADAR is mounted to the robotic arm using a combination of double sided tape, zip ties, and a c-clamp. The wires for both the web cam and LADAR are then run together with the existing robotic arm wires allowing for a neat and reliable set up. The video camera is mounted on a pan tilt mechanism, a fixed elevated distance behind the robotic arm. This allows for a broader environment scanning prior to initiating a scan by the robotic arm.

#### 5.2.2 Connecting the system components

The webcam's receives power and sends its video signal through a USB connector. The LADAR is powered using a 12v power output of an LM2677 and the output

signal is sent via a USB connector. The robot arm is then powered using the 24V power output from the battery and connected to the laptop via a USB cable.

The video camera is now powered through the 15V power output of an LM2677 and sending a signal through USB. The pan tilt is then connected in parallel, to the robot arm, to the 24V output of the battery.

Finally the USB hub is powered by the 5V output of the LM2677 and then connected to the USB input of the laptop. The laptop is powered using the 19.5V output of the LM2677.

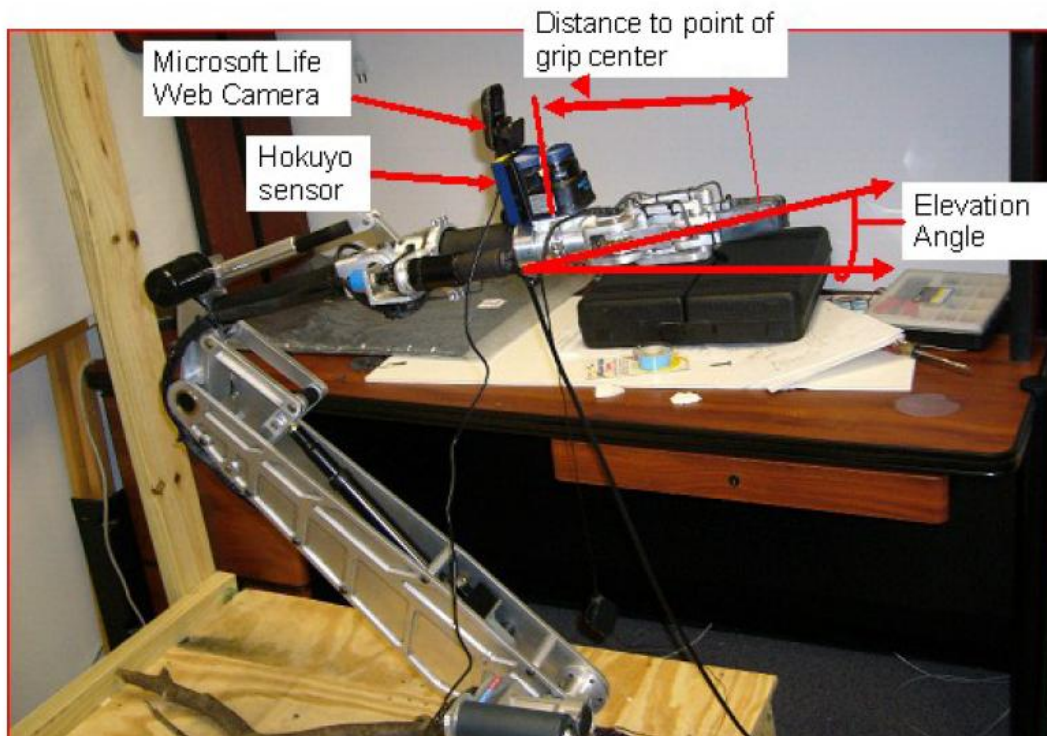


**Figure 5.1 Robot arm with attached sensors**

### 5.3 Energy system integration

The energy system is mounted alongside the robotic arm setup. The battery system is setup next to the engine along with the accompanying components. The main output from the engine alternator goes to the battery system in turn supplying the sensory system with power. The 24V output from the batteries is extended from the battery setup to the power distribution strip of the sensory system as shown in the following figure.

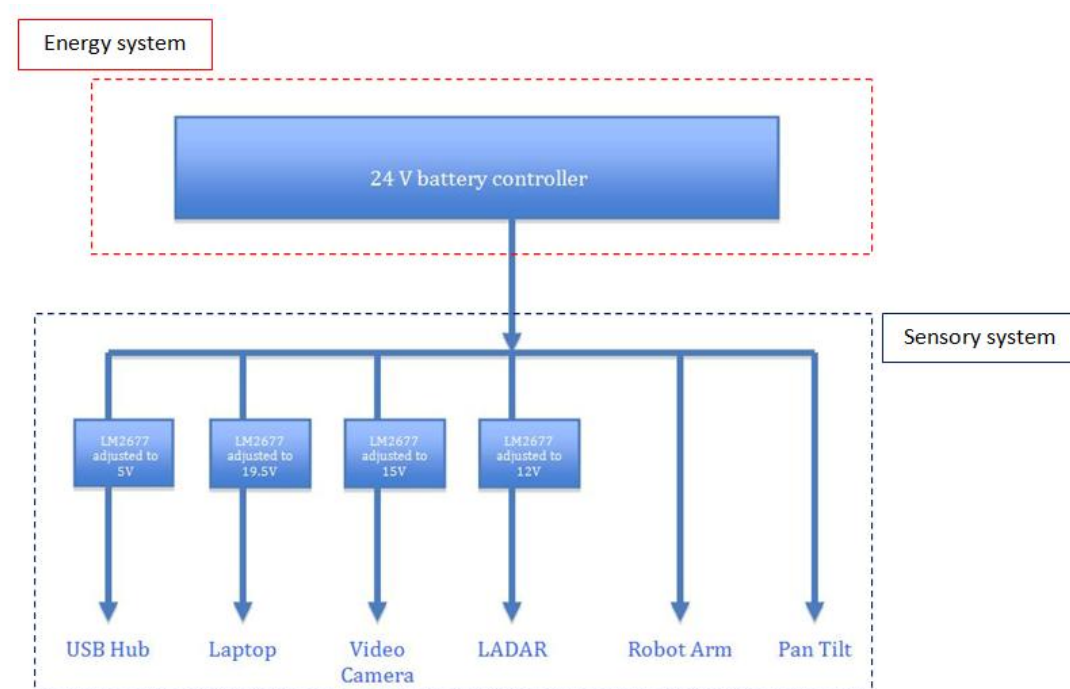


**Figure 5.2 Connecting the energy system to the sensors**

### 5.4 Control system integration

#### 5.4.1 Pellx controller adapter

As discussed previously, the pellx controller must be adapted to actively adjust to the various fuel sources. The controller allows for the adjustment of the size of the initial

starting feed, feed rate of pellets, and the fan speed. Also included is an indicator which provides a visual of how the burner is operating.

Extensive testing is done in order to manually adjust the appropriate parameters for the controller. However, electronically monitoring the system feedback and using a microprocessor to analyze the data would allow for active adjustment of the system.

In order to monitor the systems gas output an oxygen ( $O_2$ ) sensor is mounted in the exhaust fuel chamber. The function of this sensor is to measure the proportion of oxygen in the gas from combustion. With this information, the quality of the combustion is analyzed and adjusted in the case where the engine is running too rich or too lean. When the engine is running too lean, there is an excess of oxygen in the combustion and this can be adjusted for by lowering the fan speed. On the other hand when the engine is running too rich, there is a lack of oxygen in the combustion and this can be adjusted for by increasing the fan speed. These adjustments can be made using a circuit that would vary the voltage of the fan based on the incoming information from the  $O_2$  sensor.

The  $O_2$  sensor works by referencing the external air and comparing it to the exhaust gas. The greater the difference, the higher the voltage reading will read. This comparison causes a change in the resistance in the sensor which in turn causes a change in voltage. A narrow band oxygen sensor will typically generate up to about 1.1 volts when the fuel mixture is rich and there is little unburned oxygen in the exhaust. When the mixture is lean, the sensor output voltage will drop down to about 0.2 volts or less. When the air/fuel mixture is balanced or at the equilibrium point, of about 10 to 1, the sensor will read around 0.8 volts (14). An Arduino UNO board is

used to build the control system. The Arduino UNO uses an ATmega328 microcontroller and is equipped with both analog and digital inputs. To setup this system, the narrow band O<sub>2</sub> sensor is connected to the analog input of the Arduino, pin 1. This input of 0.2-1.1VDC is then converted, using the built in analog to digital converter, to a 16 bit digital signal. The signal to the fan is generated through the Arduino's digital pulse width modulated (PWM) output. Since the fan is not equipped with a PWM input, a circuit to convert this output to a smooth dc voltage is needed. This will allow the fan speed to be varied by lowering and raising the voltage. This can be achieved using the LM317 voltage regulator.

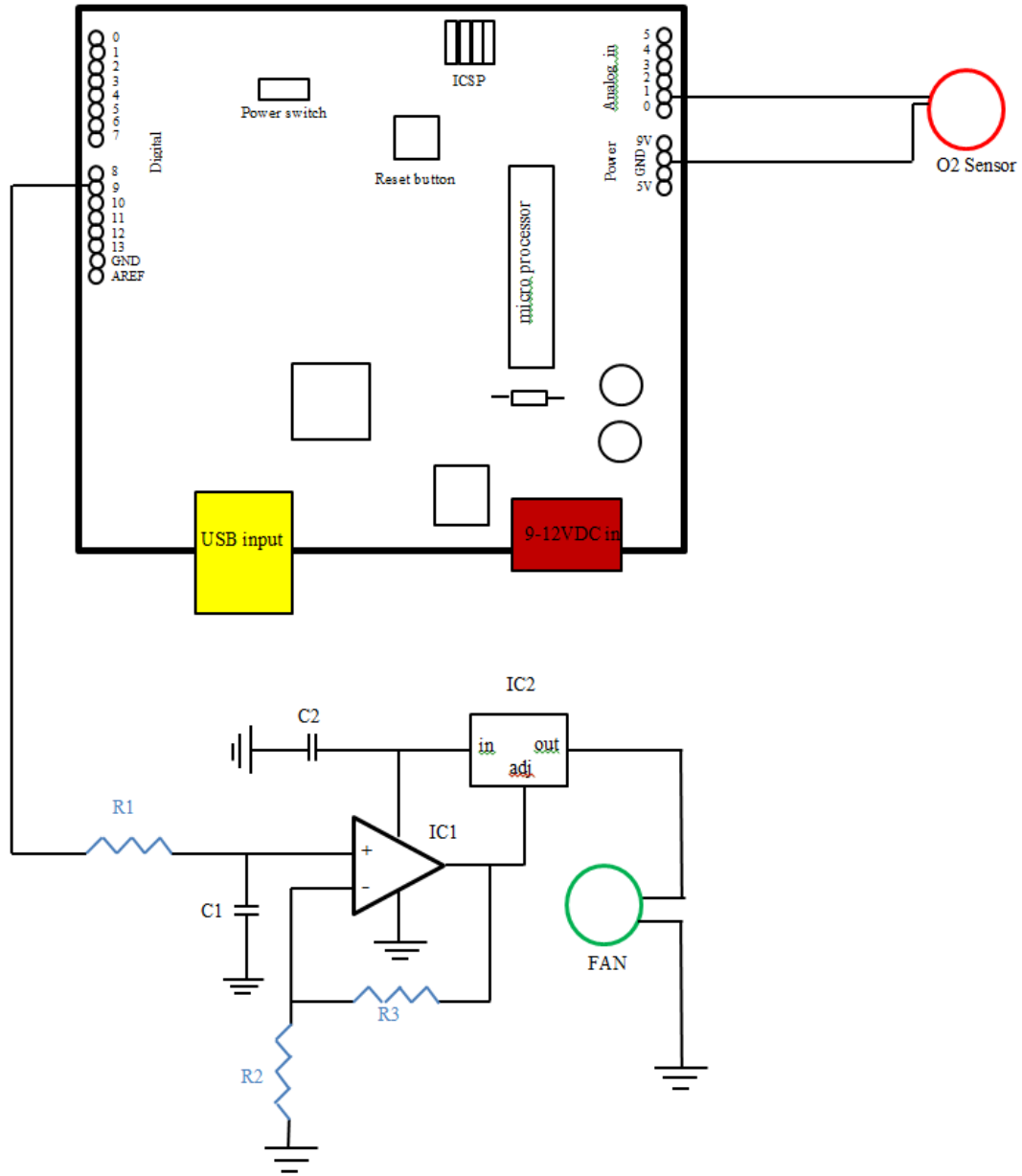


**Figure 5.3 O<sub>2</sub>/fan controller**

The Arduino code used to control the system is as follows:

```

Int O2Sensor=1           //assign the O2 sensor to analog pin 1
Int Fan=9                //assign the fan output to analog pin 9
Void setup{
Serial.begin(9600)       //set the bog rate
PinMode(O2Sensor, INPUT) //set pin 1 as an input
PinMode(Fan, OUTPUT)    //set pin 9 as an output
AnalogReference(internal) //changes reference voltage from 0-5V to 0-1.1V
}

```



```

Void loop{
Int Val=0
Val=AnalogRead(O2Sensor)/4 //read the input from the O2 sensor and divide
    If (Val<186) //by 4 in order to convert to an 8 bit input.
        Val=Val
        AnalogWrite(Fan, Val) //if the engine is running lean then decrease the
    If(Val>210) //fan speed proportionally
        Val=Val
        AnalogWrite(Fan, Val) //if the engine is running rich increase the fan
    If(Val>=186 && Val<=210) speed proportionally
        Val=0
        AnalogWrite(Fan, Val) //if the ratio is optimal don't do anything
}

```

#### 5.4.2 Fuel moisture content monitor

The moisture content of the fuel is an important property which is essential in the proper combustion of the fuel. Variation in the moisture content of the fuel will in turn result a variation of the energy content of the fuel. Wood burns best when the moisture content is less than 20%. There are two ways to measure the moisture content in the fuel. Either by directly measuring the moisture content of the incoming fuel or by deriving the moisture content from the fuel gasses (16). In order to maximize the use of the fuel's capacity, a system, which monitors the moisture content, must be implemented. Moisture from the wood dissipates into the surrounding air raising the humidity level in the storage container. A humidity sensor can sense this increase and trigger an external system to remove this added moisture. An HS-2000, analog output, temperature/humidity sensor is used. This sensor will detect the relative humidity in the canister and output a voltage directly proportional to the input voltage and percent relative humidity. This output can then be sent to a microprocessor and triggers the external dehumidification system in the case that the relative humidity exceeds the acceptable level of 20%. The HS-2000 temperature/relative humidity (RH) sensor is used to monitor the humidity level in the

storage canister. The analog output from this sensor is connected to the same Arduino board, allowing for easy, simultaneous processing. Once a RH level of at least 20% is detected, the 5V output from the board triggers an external relay to supply 12V to the fan assembly, thus dehumidifying the storage canister and drying the wood.

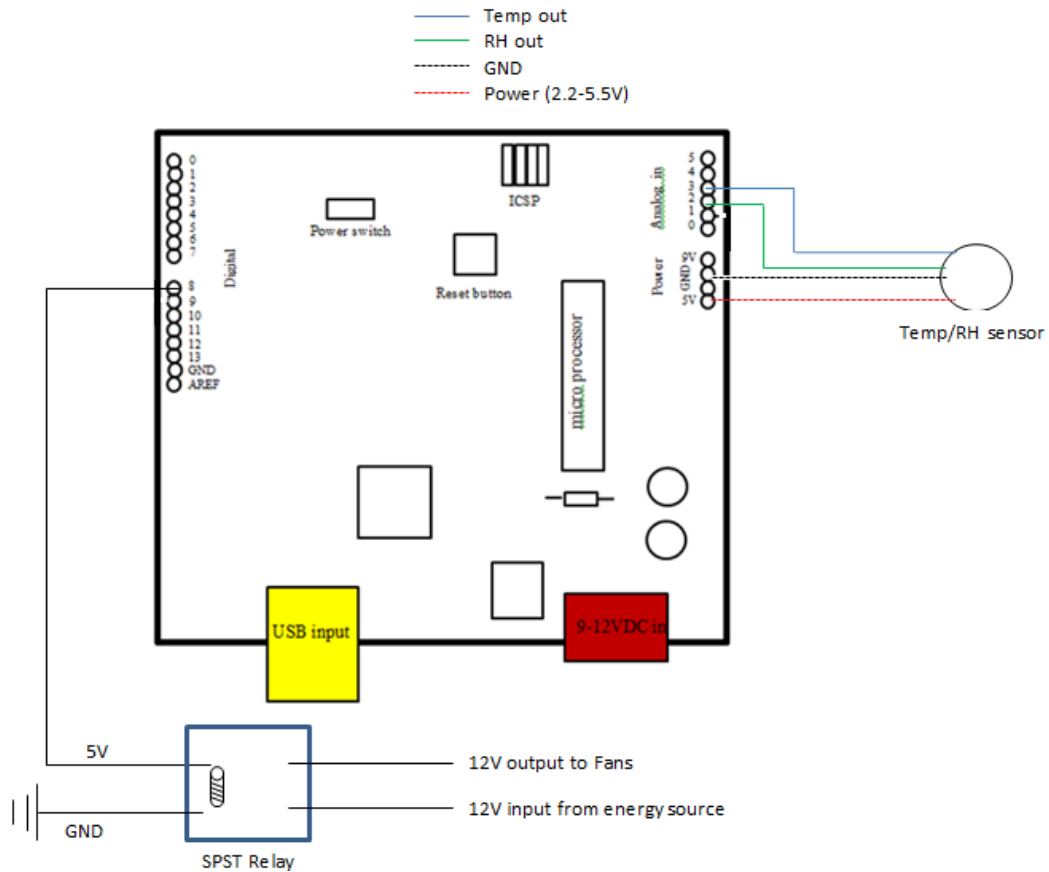


Figure 5.4 RH monitor and controller

The Arduino code used to control the system is as follows:

```

Int RHSensor=2 //assign the sensor to analog pin 2
Int Relay=8 //assign the relay to the digital pin 8
Void setup{
Serial.begin(9600) //set the bog rate
PinMode(RHSensor, INPUT) //set pin2 as an input
PinMode(Relay, OUTPUT) //set pin 8 as an output
}
Void loop{
Int Val=0
Val=AnalogRead(RHSensor) //read the input from the RH sensor

```

```

    If (Val>=410)           //a 20% humidity level is equivalent to 410 on
    Val=High               the 16 bit scale
    DigitalWrite(Fan, Val) //turn on the digital pin to high (5V output)
    If(Val<410)
    Val=Low
    DigitalWrite(Fan, Val) //if the humidity is less than 20% set the digital
}                          output to low (0V)

```

There are two ways to remove moisture from the air. The first involves running this air through a chiller, which then removes the moisture by condensation. The second can easily be achieved by conveying the air through a desiccant, such as silica gel. Silica gel can absorb and contain water up to 40% of its weight and is the most absorbent desiccant on the market today (17). The first approach would require the use of a condenser, pump, coolant and fan thus creating a more complex, energy hogging system. The second approach would only require a fan and the selected desiccant. The only concern would be an unrealistic required amount of desiccant needed to achieve reasonable operation. To calculate the required amount of desiccant needed the following assumptions are first made:

- The average density of the wood being stored is  $\sim 600 \frac{kg}{m^3}$ .
- The storage container has a volume of  $1ft^3=0.0283m^3$ .
- The full storage container would only contain 90% wood (by volume) as the rest would be considered a small gap.
- Silica gel, the selected desiccant, can hold water up to  $\sim 40\%$  of its weight.
- The incoming wood has a moisture content of  $\sim 35\%$ .
- Acceptable moisture content for wood to be burned is 20%.

From the following assumptions, the actual weight of the wood in the canister is calculated.

$$600 \frac{kg}{m^3} (0.0283m^3)(0.9) = 15.28kg$$

The actual weight of wood, occupying the  $0.0283m^3$  storage container, is  $15.28kg$ .

With a moisture content of ~35%

$$15.28kg(0.35) = 5.35kg$$

There is approximately  $5.35kg$  of moisture in the storage container. A moisture level of 20% is acceptable.

$$15.28kg (0.20) = 3.05kg$$

$$5.35kg - 3.05kg = 2.3kg$$

$2.3kg$  of moisture needs to be absorbed by the desiccant. Silica gel can hold up to 40% of its weight in absorbed moisture.

$$xkg(0.40) = 2.3kg$$

$$xkg = \frac{2.3kg}{0.40} \Rightarrow x = 5.75kg$$

This desiccant can be spread out over the surface area of the storage canister. This result is compared to commercial dehumidifiers. In order to achieve similar results a  $75W$ ,  $\$70$ ,  $1.3pint/day$  ( $\sim 0.615kg$ ) removal dehumidifier is required.  $75W$  is about 16% the current power requirement of the entire system. Hence, using a dehumidifier would be highly impractical (18). The disadvantage of using desiccant is that it would have to be recharged once the maximum moisture capacity has been absorbed. This can be achieved by heating the silica gel at  $250^{\circ}F$  for 2 hours (19).

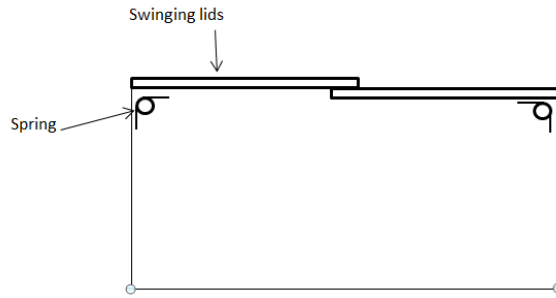


**Figure 5.5 Side view of the storage canister lid**

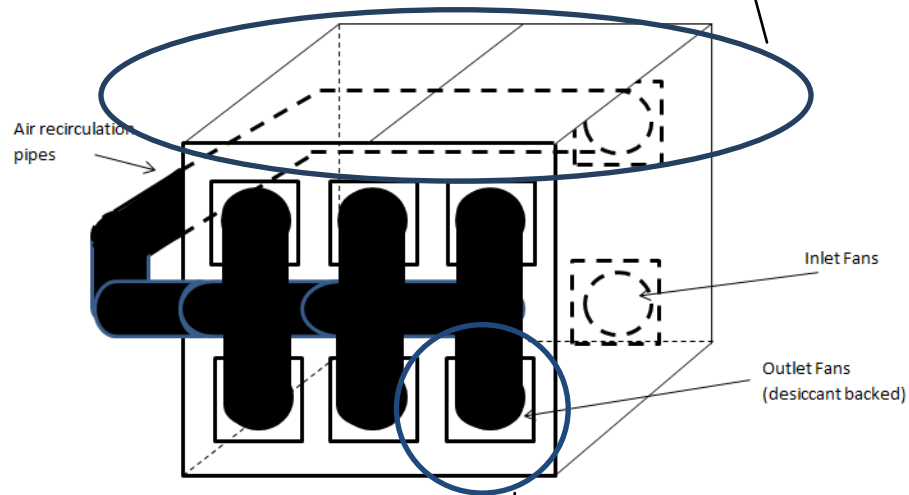


**Figure 5.6 Storage canister with dehumidifying system**

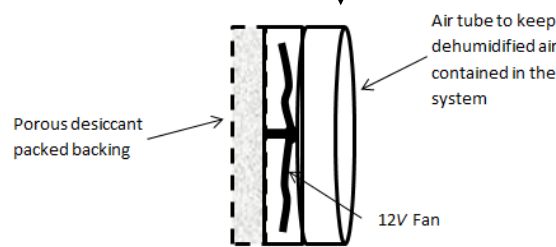


**Figure 5.7 Side view of fan setup**

The dehumidification system will be comprised of desiccant packets and fans placed along the wall of the storage canister. A recirculation system redirects the dehumidified air back to the rear fans to be pumped back in and a spring loaded cover will be used to keep the storage canister sealed while still allowing the arm to drop wood in.

## **Chapter 6: Results**

### 6.1 Introduction

After integration of the system, the capabilities were tested and evaluated. The goal of the system at this point was to be able to scan objects in an environment, accurately distinguish that which are biomass and calculate the inverse kinematics. Various tests were run and evaluated. The details encompassing this process are discussed in the following chapter.

### 6.2 LADAR results

#### 6.2.1 Hokuyo software

The LADAR is first tested using the supplied Hokuyo software. This software generates and logs data associated with the needed ranges and angles. This data can then be exported into MATLAB to be used with the image processing code. An image capture of the LADAR's view is shown in the following figure with an overlay of the reference coordinate system.

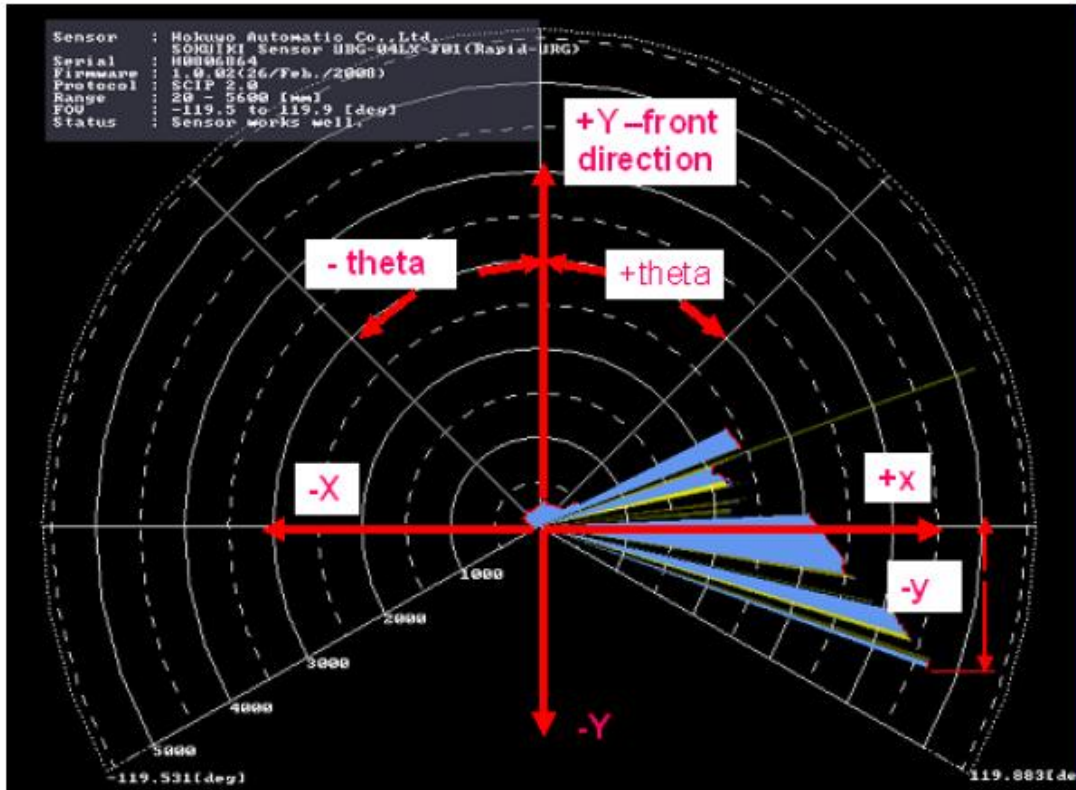


Figure 6.1 LADAR output (26)

### 6.2.2 Integrated with MATLAB

The second test incorporates the integration of the Hokuyo LADAR with MATLAB. The LADAR is now oscillated up and down in order to acquire a 3D data representation of the visible space. This data, once imported into MATLAB, can be plotted using a 3D mesh which shows a more accurate illustration of the target area.



Figure 6.2 Target area to be examined (26)

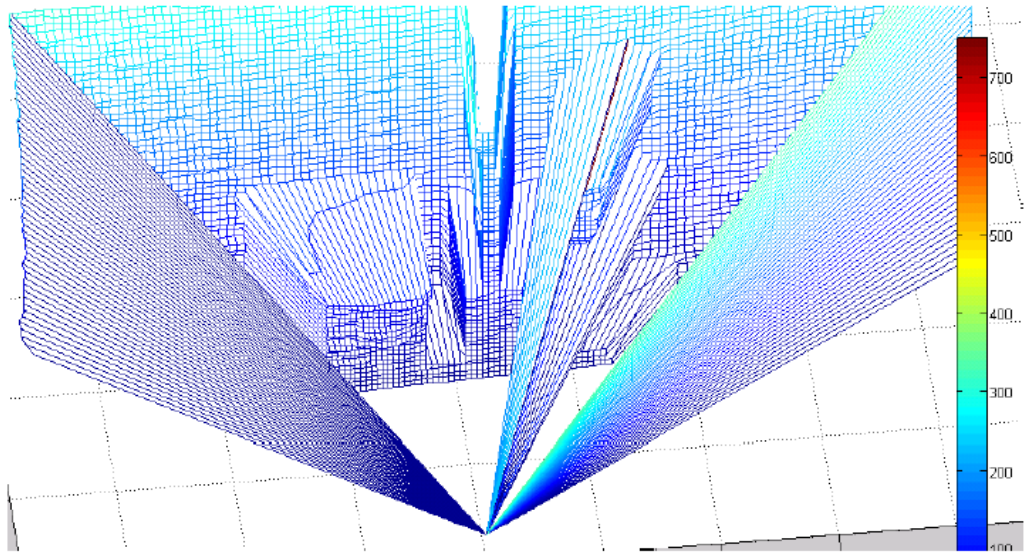
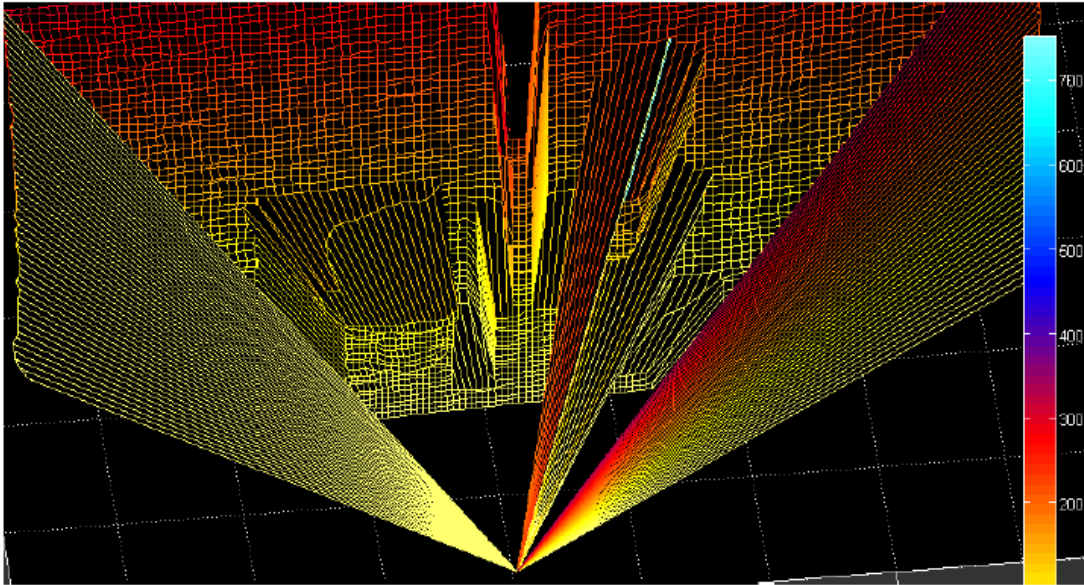


Figure 6.3 3D representation of the target area (26)



The 3D representation of the target area is shown in figure 37. Once imported, this data is simple to manipulate. The inverse and the reverse of the above plot are also shown.



**Figure 6.4 Inverse of the 3D image (26)**

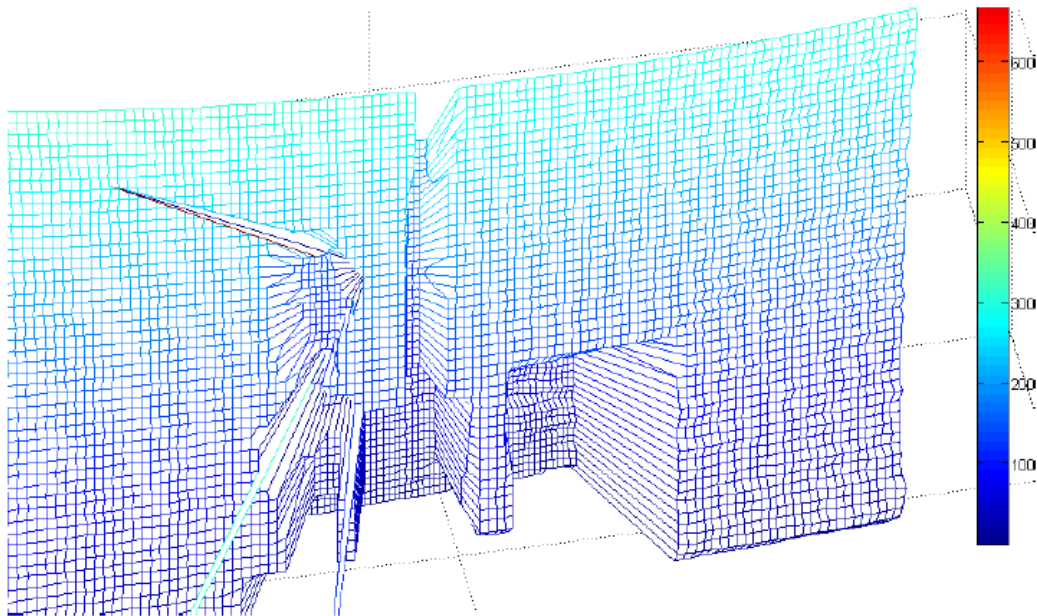


**Figure 6.5 Reverse of the 3D image (26)**

### 6.3 LADAR and webcam results

The test is then run using both the LADAR and webcam in conjunction with MATLAB and C#. The robotic arm is moved from position N to position 1, targeting a tennis ball, as shown in the following figure.

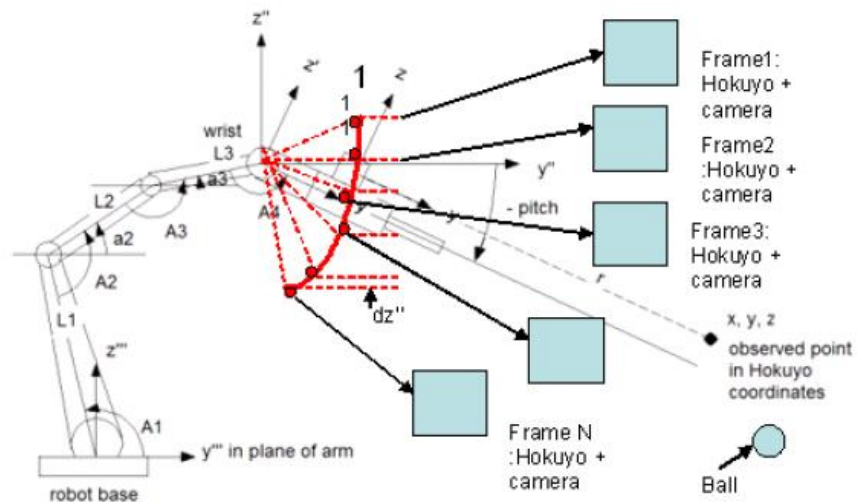
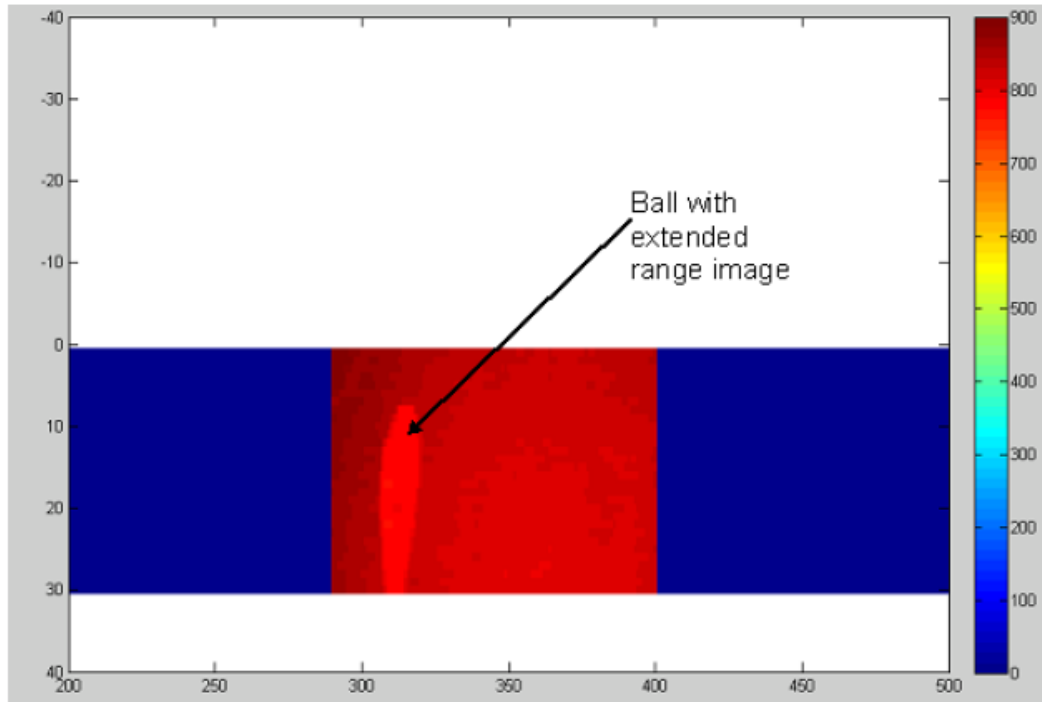


Figure 6.6 Motions of the robot arm for target frame (26)

#### 6.3.1 Single object target

The first test involved using only a single tennis ball in the target area. The scan results are obtained and processed automatically. Figure shows the results of this test.



**Figure 6.7 Image of scanned tennis ball (26)**

Due to the complex motion of the robotic arm, the image of the tennis ball appears distorted. This distortion is solved by adjusting the range of plot.

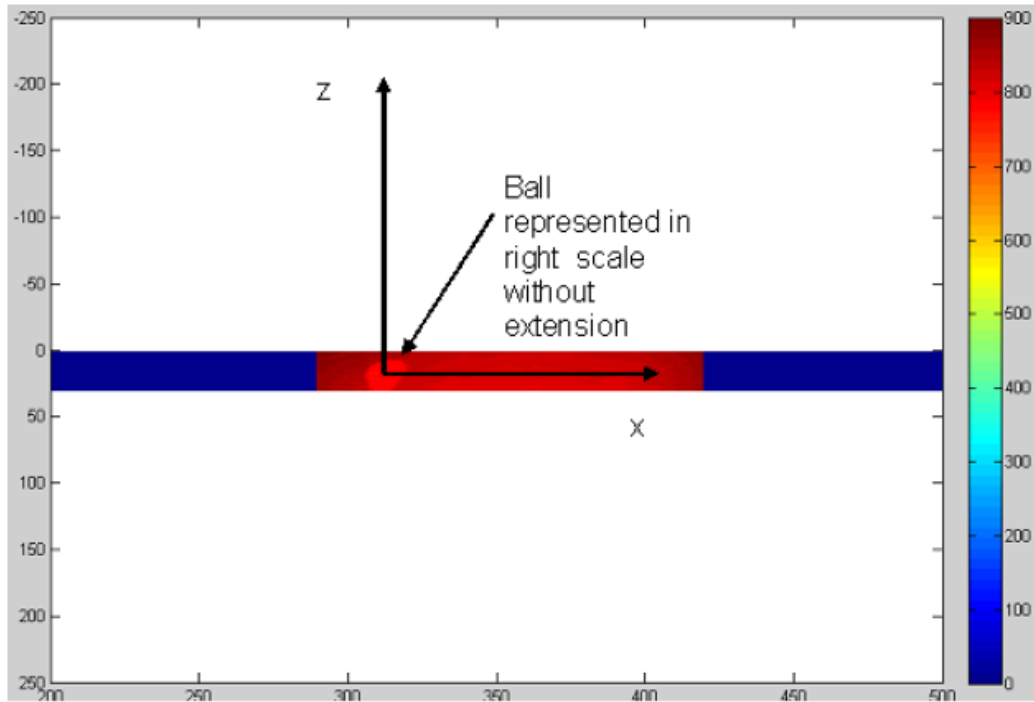


Figure 6.8 Adjusted scale for tennis ball representation (26)

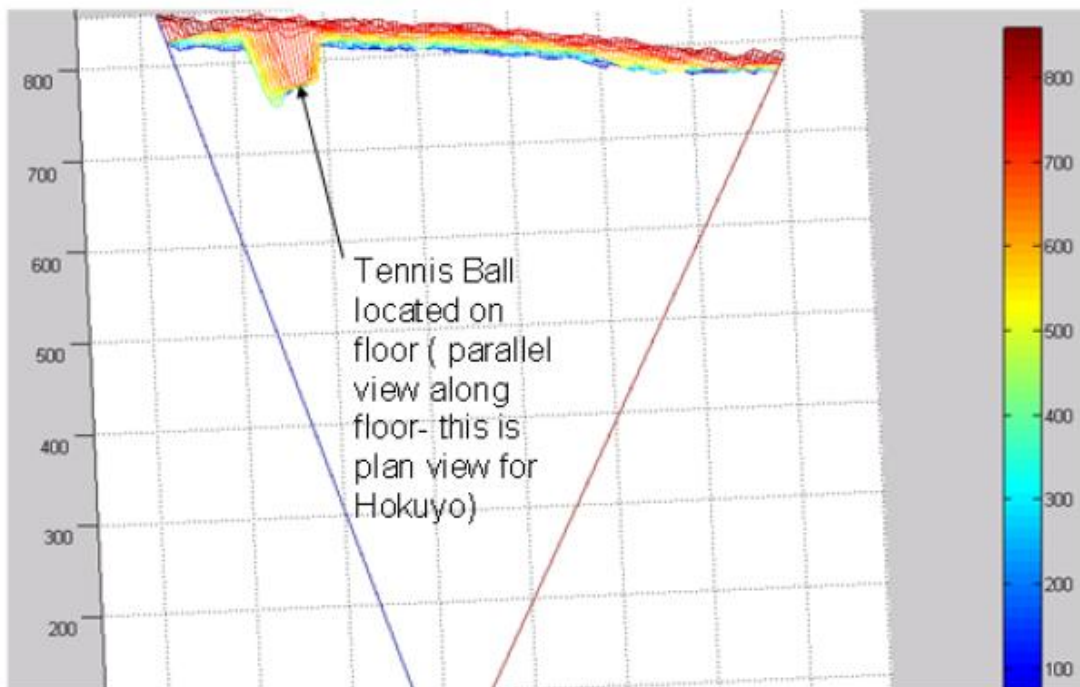
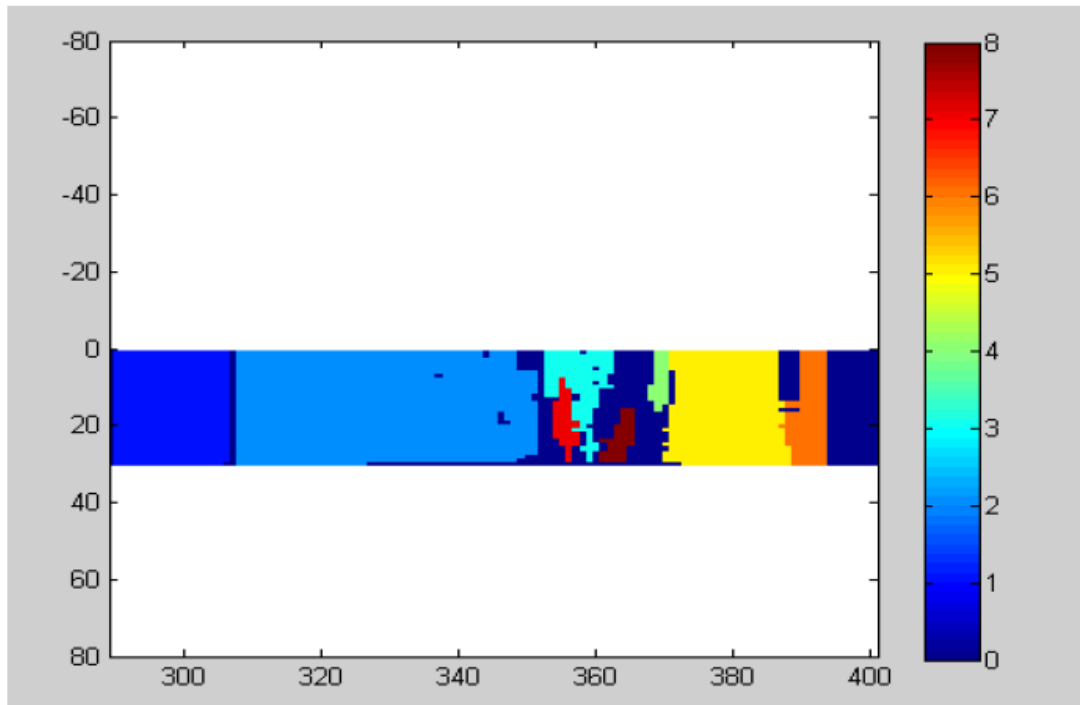


Figure 6.9 3D representation of tennis ball (26)

### 6.3.2 Multi object target

Additional objects are now added to the target area as shown in figure 6.10. The scanning path for the robotic arm is kept the same however. Due to the complexity of the various geometries it is more difficult to establish an accurate range differentiating the objects.



**Figure 6.10 Multi object capture of target area (26)**

### 6.3.3 Watershed method for multiple objects

Analysis of the previous figure demonstrates that in order to accurately differentiate between biomass objects additional criteria must be introduced. For this, the watershed approach is introduced. This allows for the calculation of the object sizes and their centroids.

The first step is to use the gradient magnitude as the segmentation function.





Figure 6.11 Step 1 taking the gradient magnitude (26)

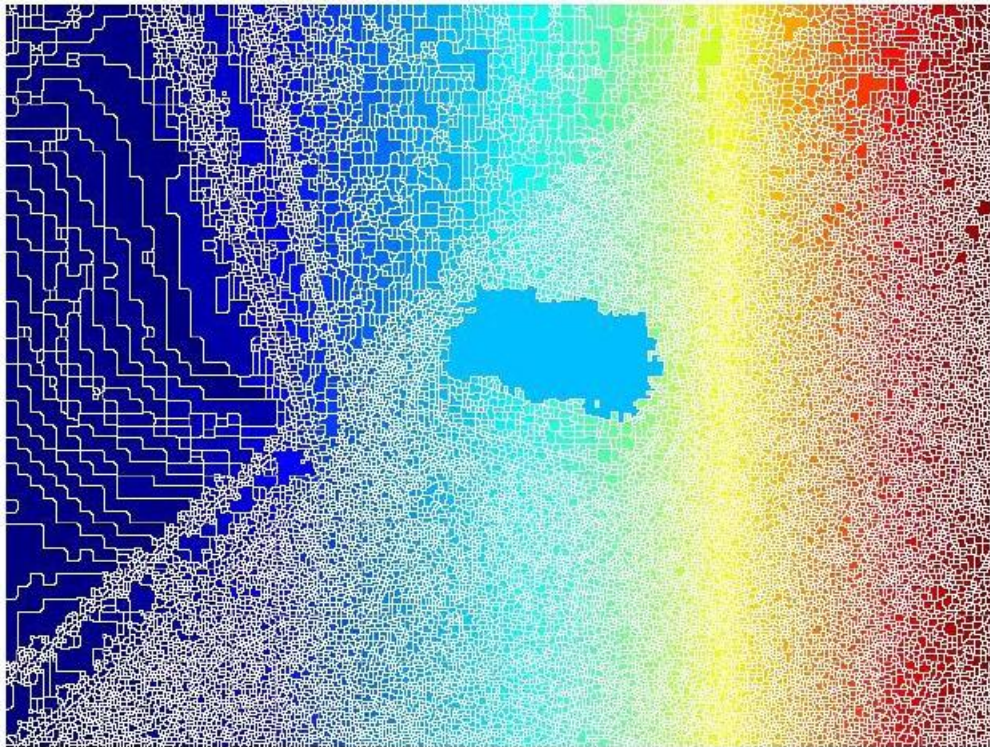
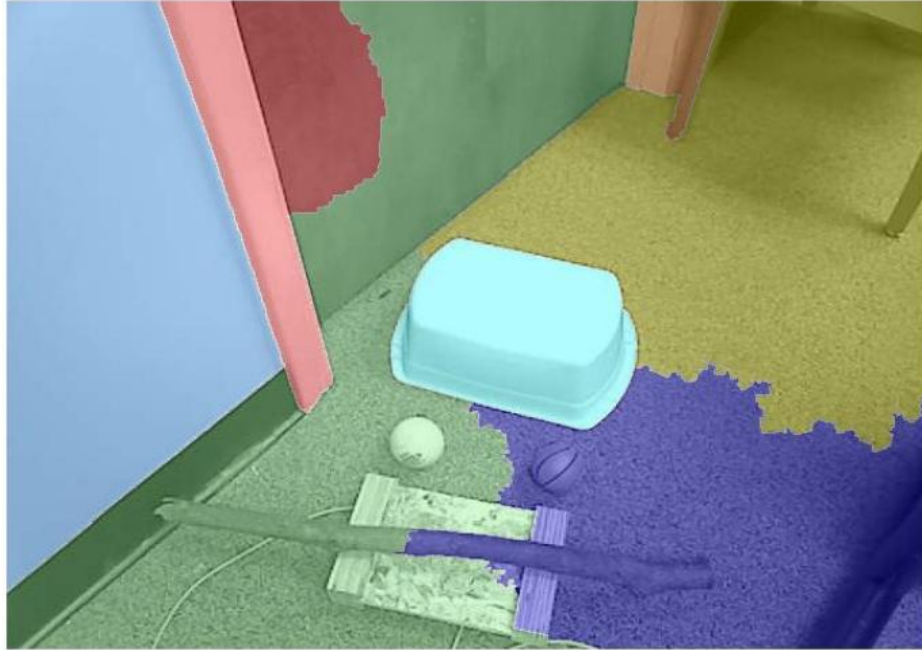
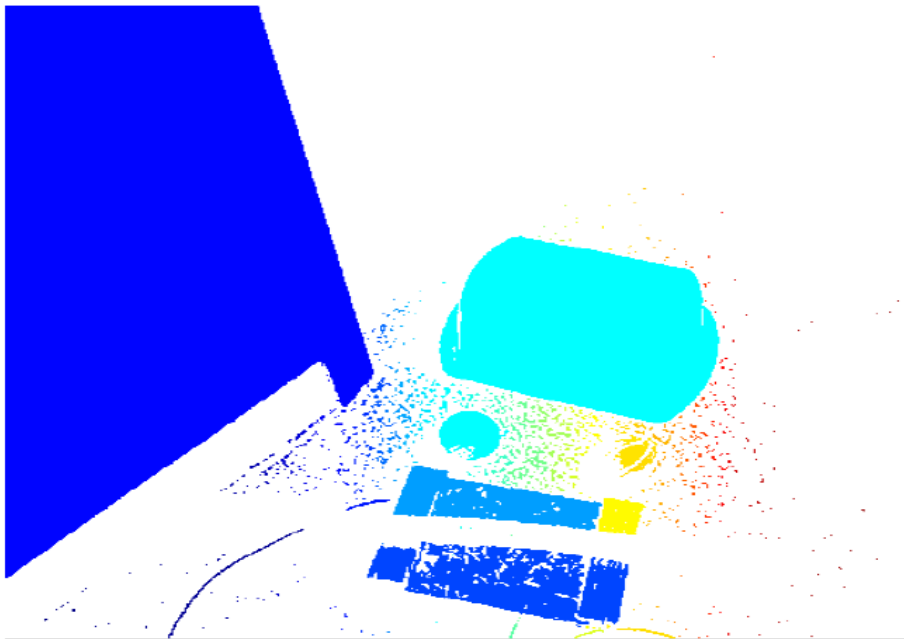


Figure 6.12 Step 2 segmenting the image using the watershed transformation (26)

Watershed transformation cannot be directly applied to the gradient magnitude since this often results in over segmentation, hence opening and closing by reconstruction is first used to filter the image.



**Figure 6.13 Step 3 transparently superimposing Lrgb on the original image (26)**



**Figure 6.14 Step 4 cleaning up the selected color segments (26)**



Figure 6.15 Step 5 of determination of the centroids watershed approach (26)

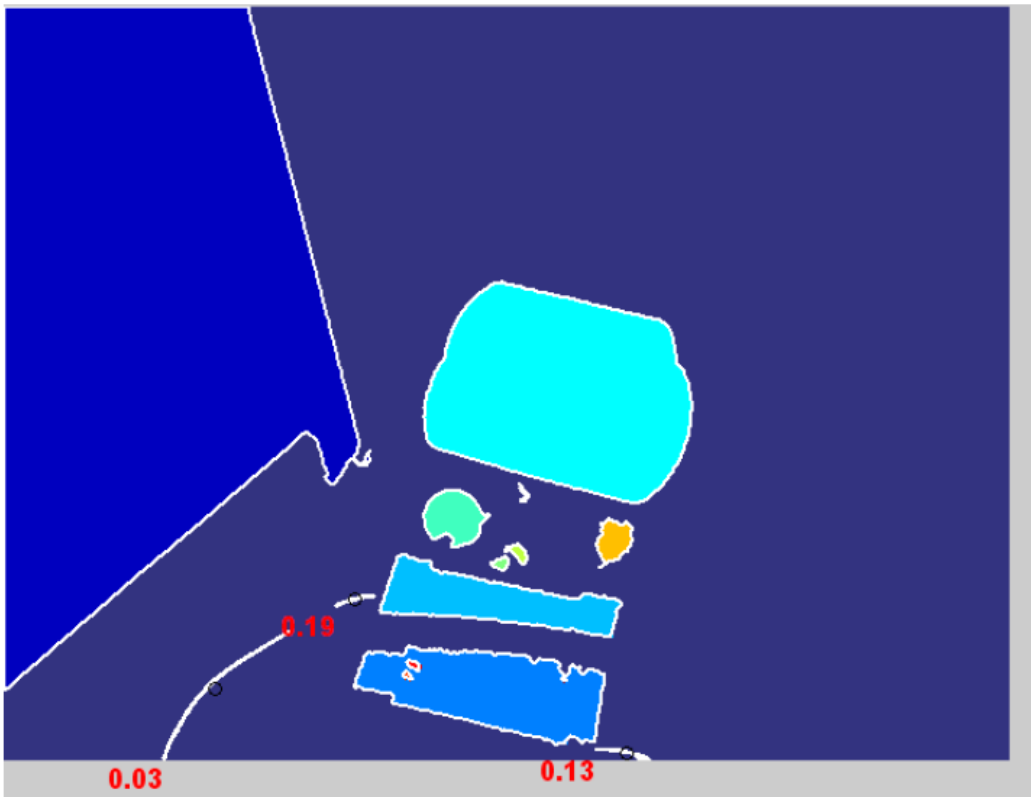


Figure 6.16 Step 6 calculating the k values (26)



As shown, differentiation between objects and calculation of centroids is achievable. The next phase involves recognizing biomass and calculating inverse kinematics in order to adequately pick up the biomass and deliver it to the engine.

#### 6.4 Determining inverse kinematics

In order to effectively grab the candidate object and deliver it to the engine, the system must be able to recognize the location of the object with respect to its relative coordinate system. With the LADAR and webcam mounted a fixed distance from the robot arm grasper the coordinates can be easily translated from the reference frame of the LADAR to that of the grasper. The biomass drop off point is mounted a fixed distance away from the robot arm. Once the object has been grasped, the robotic arm is commanded to always take the same path back to the fixed drop off point.

##### 6.4.1 Inverse Kinematics calculation for a single object

The first step involved placing a single tennis ball on a chair and obtaining the coordinates of the ball with respect to the robotic arm.



**Figure 6.17 Tennis ball to be captured (26)**

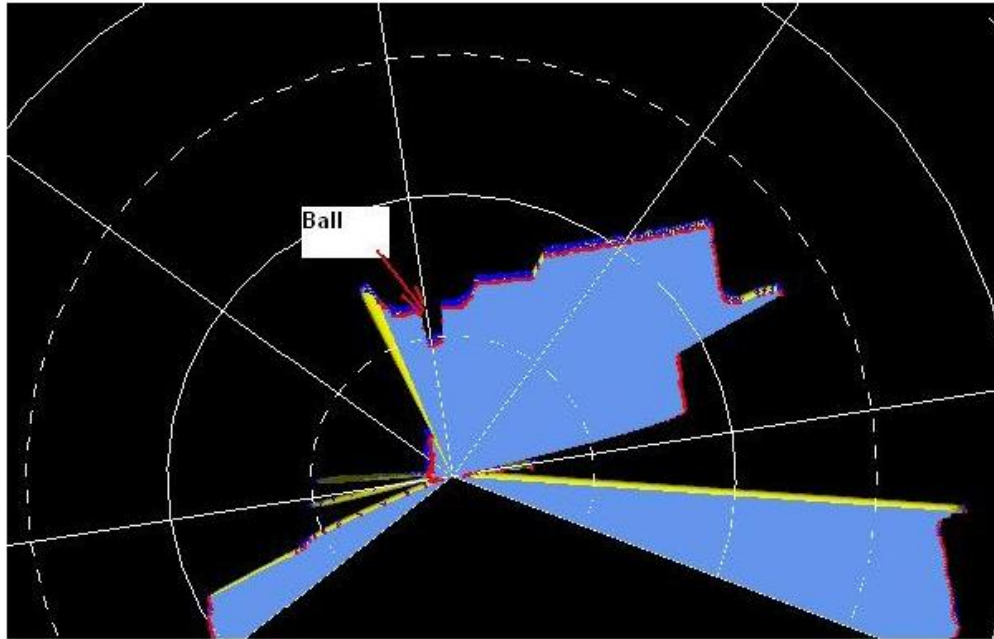


Figure 6.18 Ladar image of tennis ball (26)

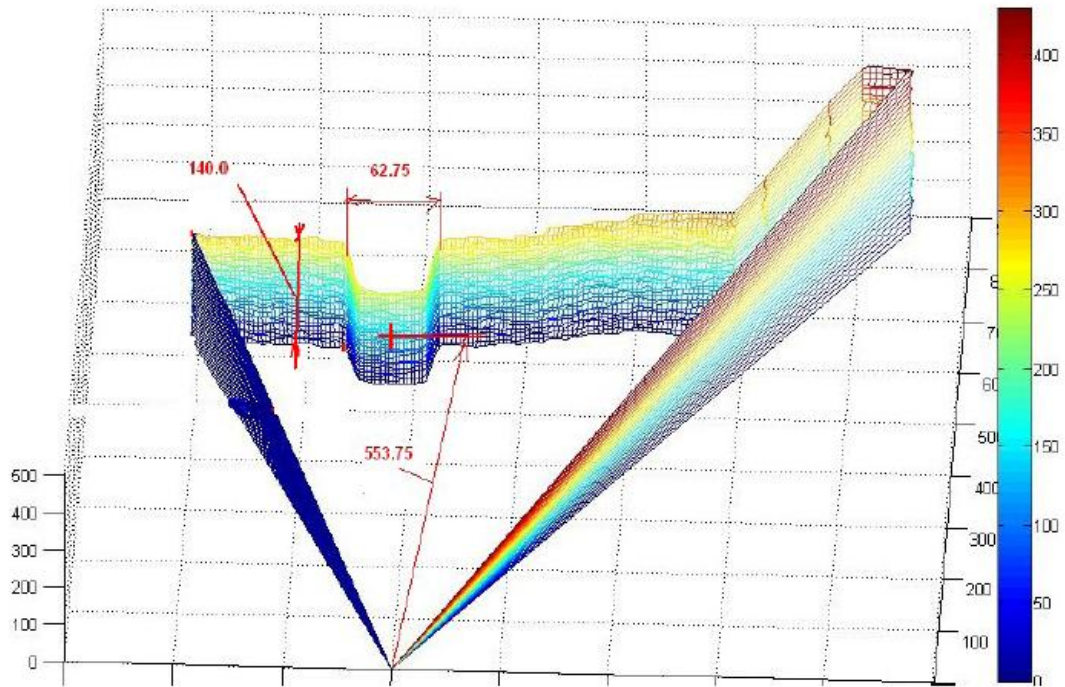


Figure 6.19 3D image of tennis ball (26)

Scanning results are shown to accurately distinguish the location of the tennis ball. However when analyzing the image more closely, there appear to be a couple of background pixels at the edge of the object as shown in figure 6.20. For a more accurate representation these borders must be filtered by eliminating very small objects in the output file.

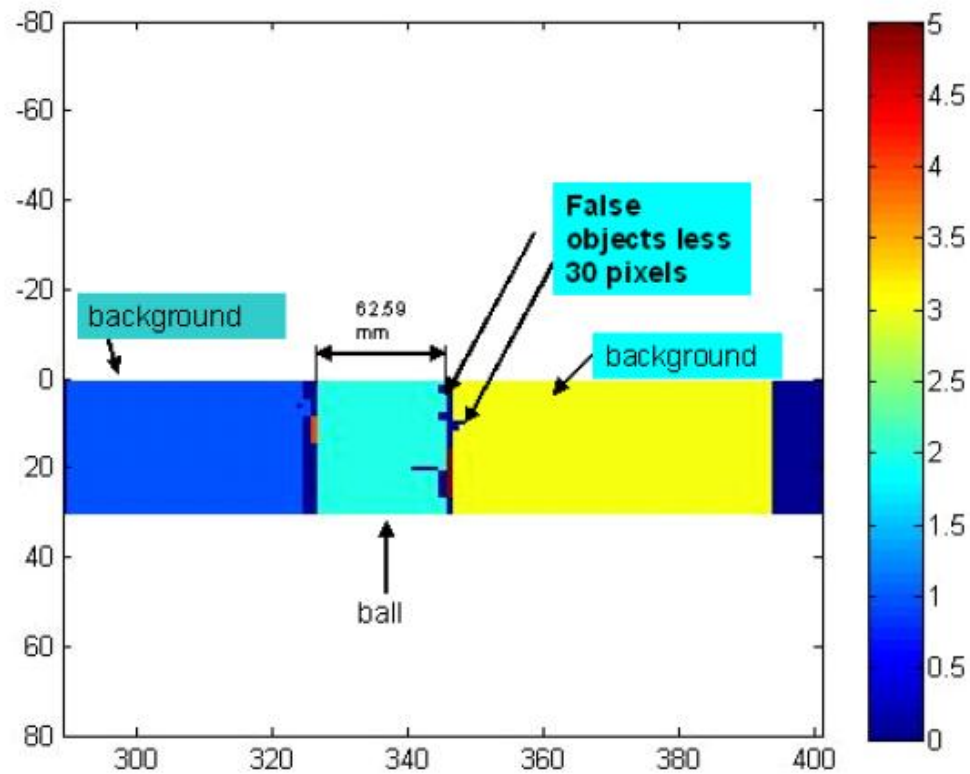
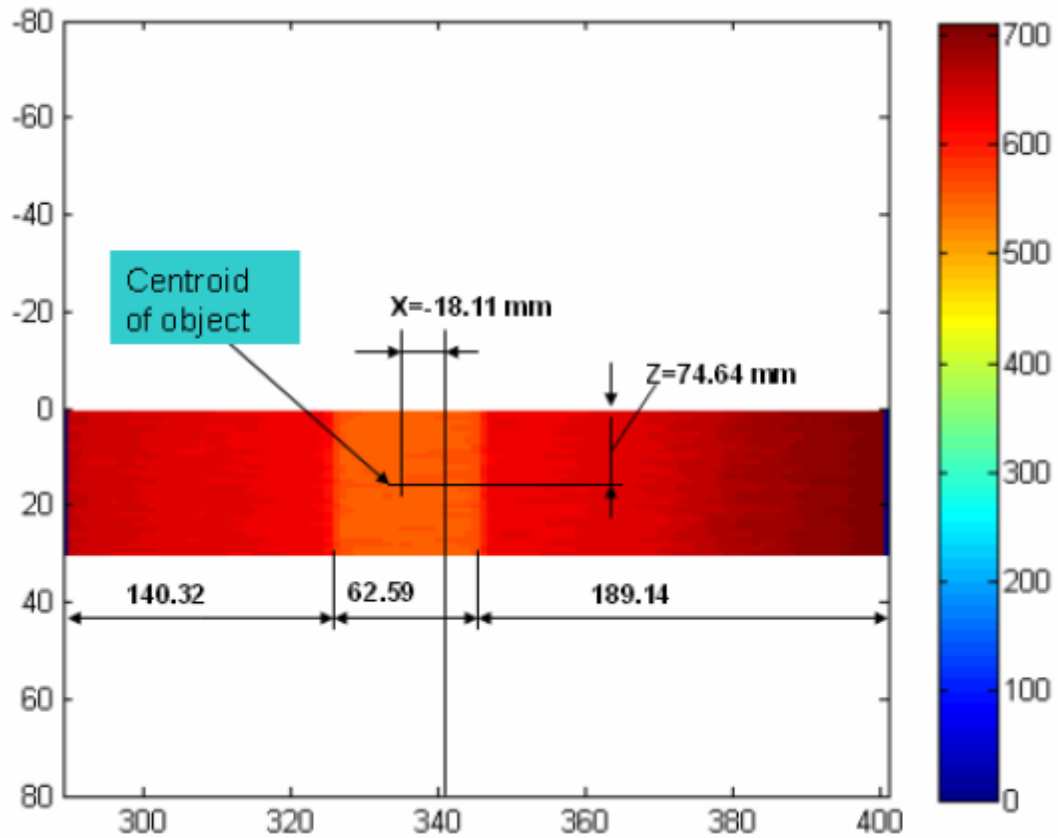


Figure 6.20 Before elimination of the very small files (26)



**Figure 6.21 Distinguishing between objects to find the centroid (26)**

From the results above it is shown that the image processing technique is effective in calculating the inverse kinematics for one object.

#### 6.4.2 Inverse kinematics calculation for two objects

The same experiment was conducted on two tennis balls.

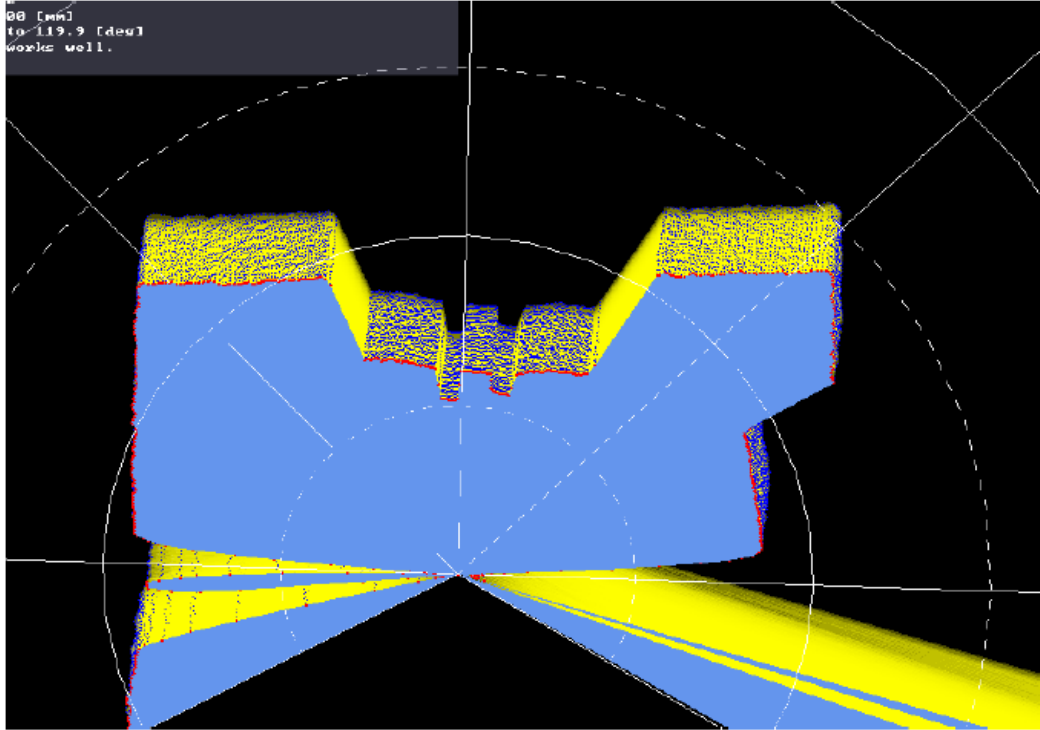


Figure 6.22 LADAR result for multiple objects (26)

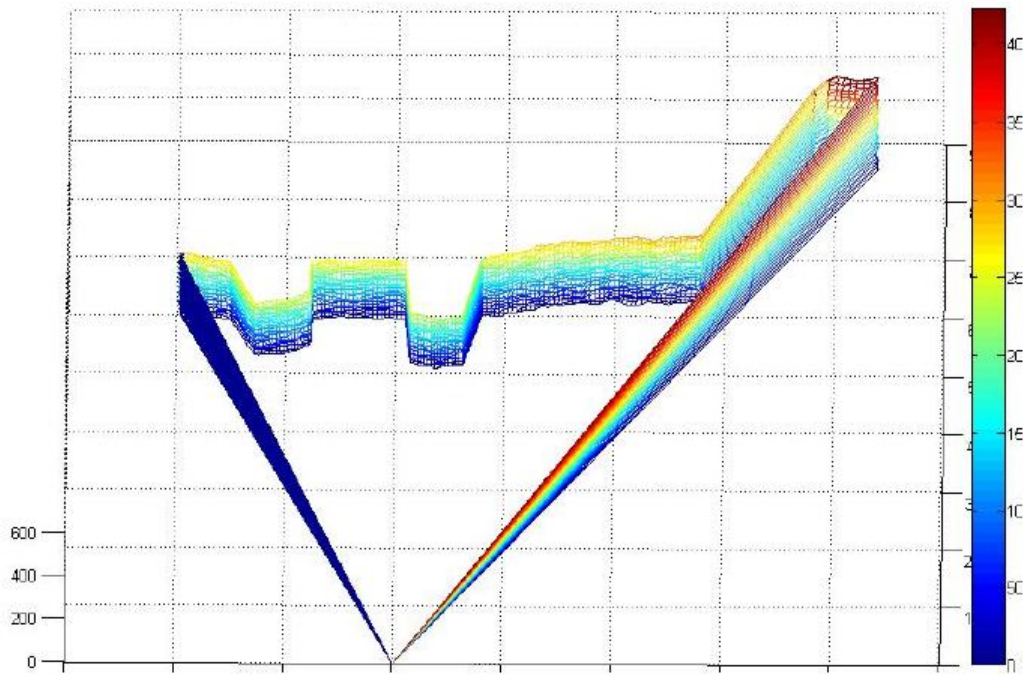
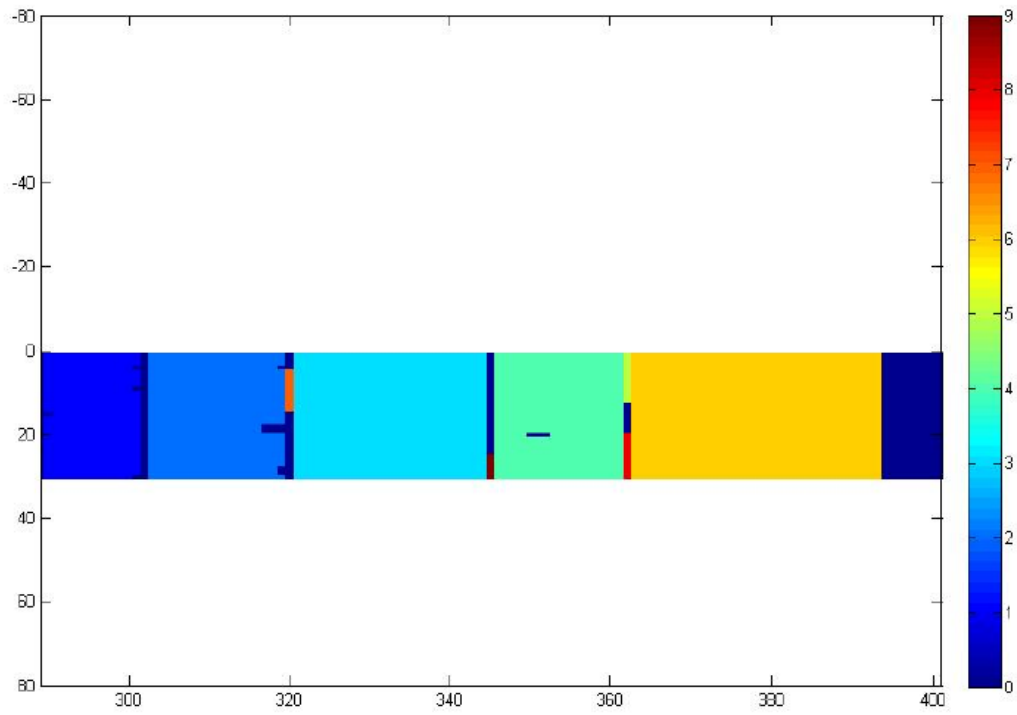
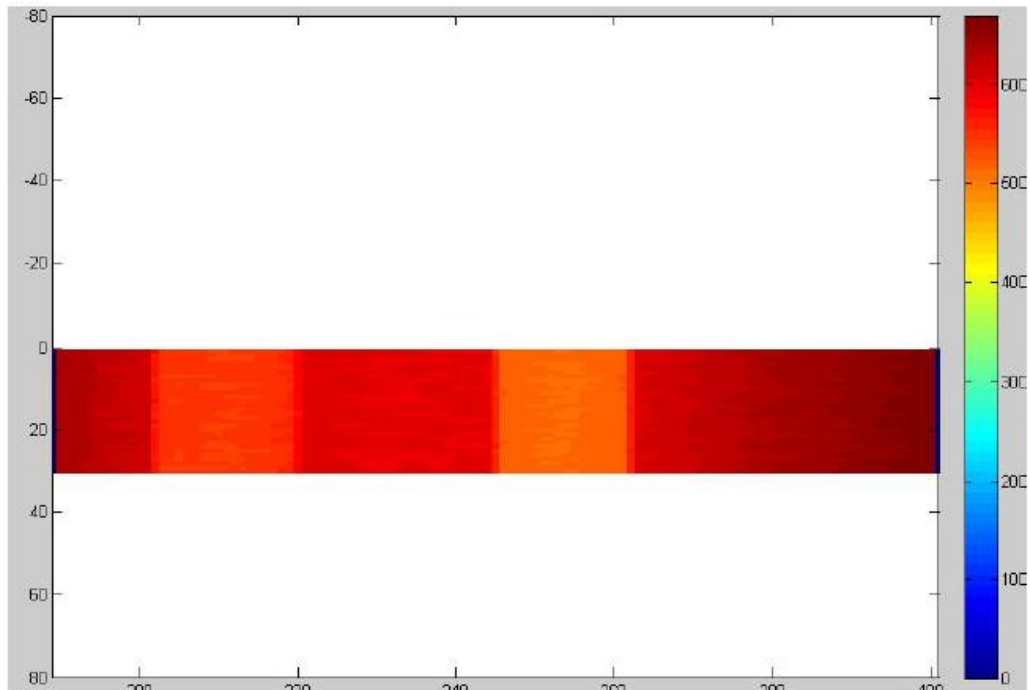


Figure 6.23 3D representation for multiple objects (26)



**Figure 6.24 Representation after eliminating the very small objects (26)**



**Figure 6.25 Centroid calculation for multiple objects (26)**

Similar to the results obtained from the single tennis ball experiment, the inverse kinematics are obtained for both tennis balls.



### 6.4.3 Inverse kinematics for multiple objects

As a final experiment, three tennis balls were placed on the chair then scanned in an attempt to calculate the inverse kinematics of multiple objects in the scene.

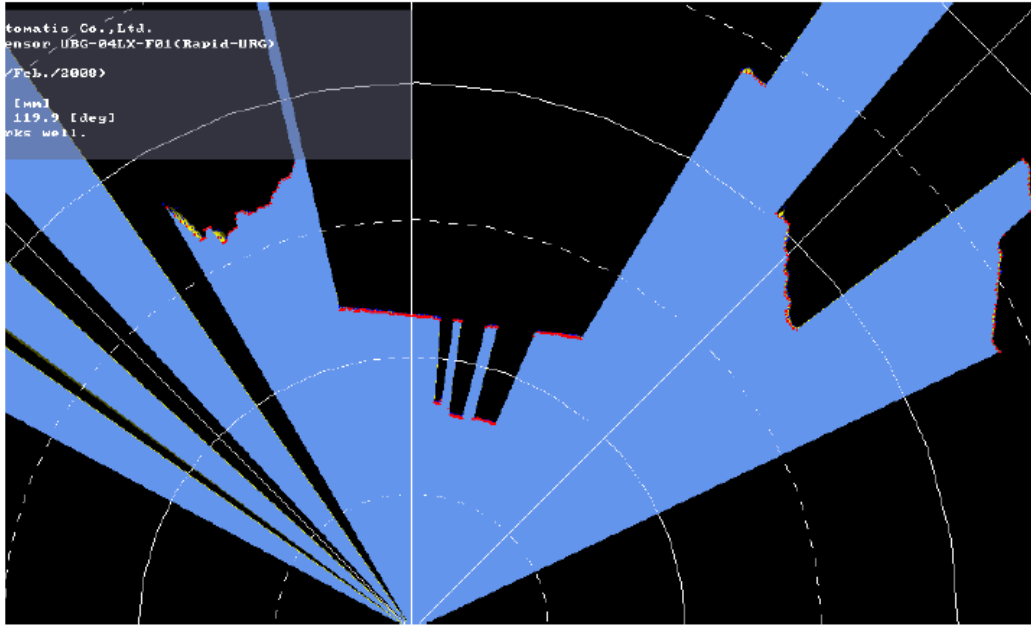


Figure 6.26 LADAR scan for multiple objects (26)

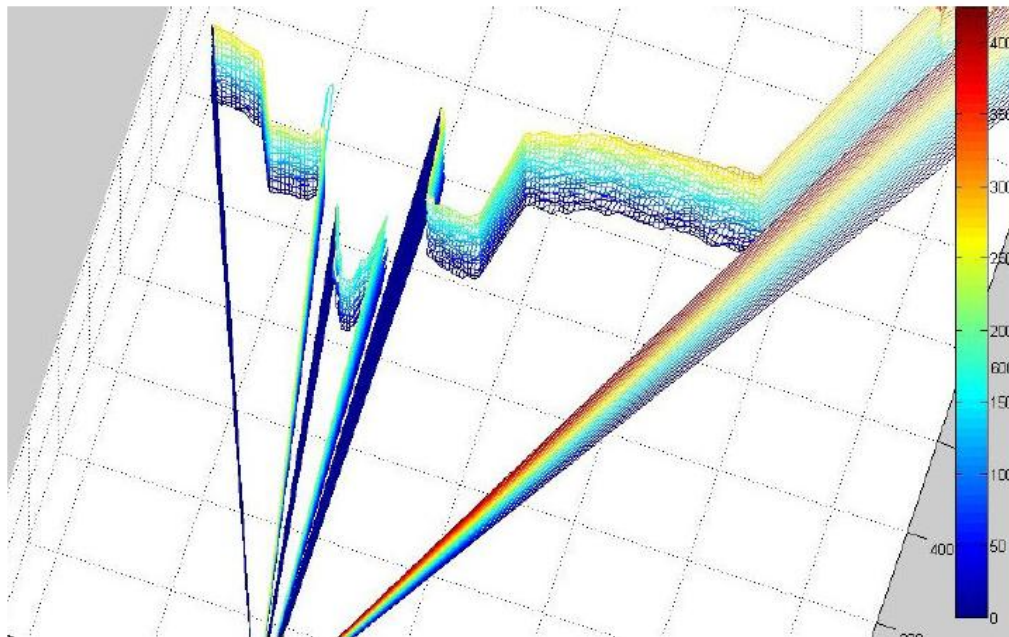
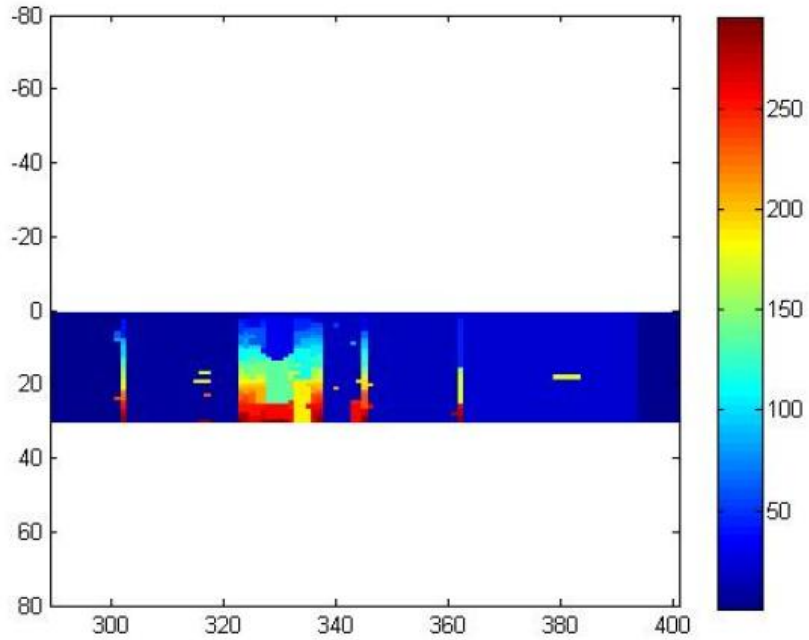
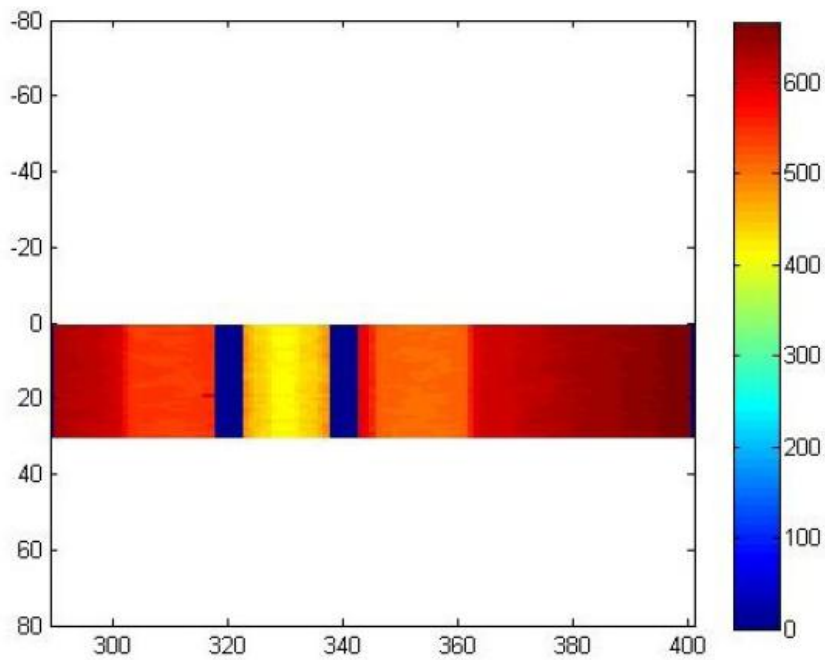


Figure 6.27 3D representation of target area (26)



**Figure 6.28** Image with the very small files attached (26)



**Figure 6.29** Image after eliminating the very small files (26)

From the final experiment it has been shown that multiple objects are able to be differentiated and a calculation of the inverse kinematics is achievable.



## 6.5 Distinguishing between biomass

### 6.5.1 Controlled environment

A multi object scene is created including both biomass and non-biomass objects.

Objects 2, 4 and 5 are biomass whereas objects 1, 3 and 6 are not. After scanning the scene a converted grayscale image is derived and the gradient magnitude, based in the Sobel operator is taken. Then the morphological technique “opening by reconstruction” and “closing by reconstruction” is taken in order to “clean up the image” (25).

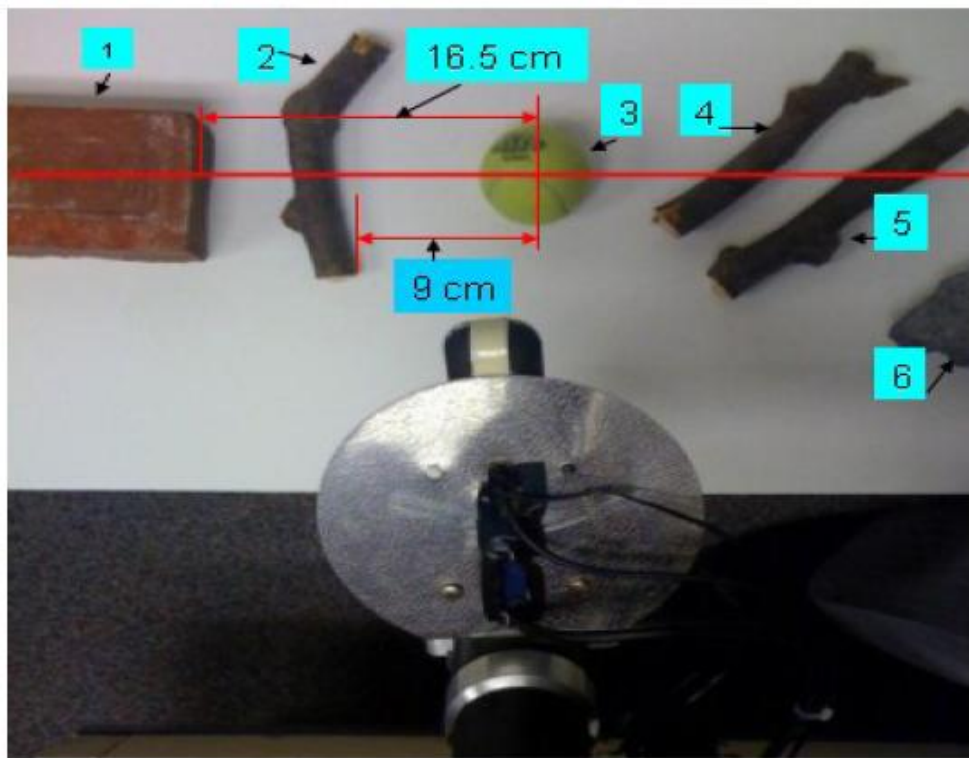


**Figure 6.30 Test area for biomass distinction (26)**

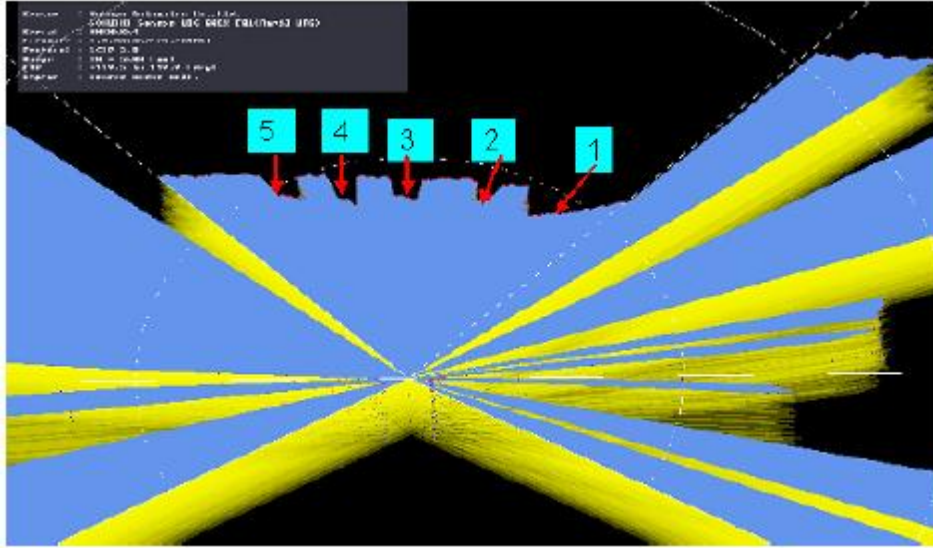


Figure 6.31 LADAR representation of the results (26)

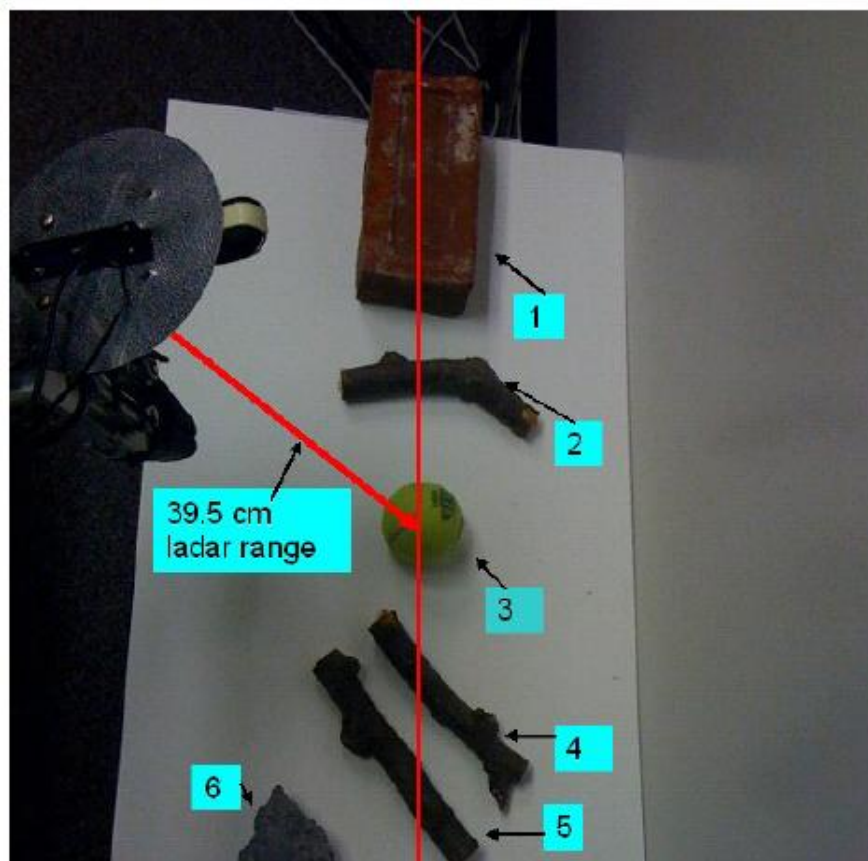


Figure 6.32 Side view of the target area (26)



Figure 6.33 Gradient magnitude of the image (26)



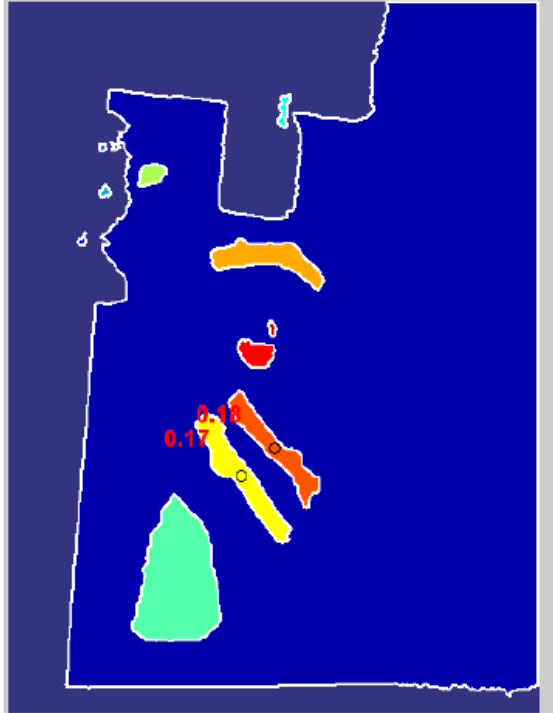
Figure 6.34 Image after “opening-by-reconstruction” and “closing-by-reconstruction” techniques (26)



Figure 6.35 Comparison of threshold “opening/closing-by-reconstruction” (26)

Similar components are grouped in the multi object scene and the Sobel edge mask is used to calculate the gradient magnitude. The gradient is high at the edges and low within the objects. This is due to the continuity within an object opposed to the discontinuities at the edges (27). Grouping objects allows for the distinction between like objects and those that are not of the same criteria. This involves labeling each pixel and referencing it to the entity to which it belongs. The entity class and properties are defined and used to distinguish between the memberships of entities. The process of classification is used to compare the various entities to the properties of the class hence allowing the assignment of the entity to a certain class or group. Also included in the image processing toolbox is a function, region groups, which allows for the extraction of an objects area, perimeter, centroid, etc. This function is useful in identifying shapes and volumes of objects.

The system will keep a library of properties defining biomass. After the image processing routine is complete, the groups will be compared to the library of biomass properties in order to define what is acceptable. In this case the simple property of the ratio between the area and perimeter, the k factor, is used. If this factor is less than 0.25 than the object is declared bio-mass and else rejected. From figure 6.36, it is seen that two objects have been shown to have k factors less than 0.25 so the robotic arm is ordered to grasp and dump them into the canister.



**Figure 6.36 Finding the k factors of the objects (26)**

#### 6.5.2 Real environment

The same experiment is now conducted outside in an actual environment. The following image of a stone surrounded by leaves is analyzed using the known techniques.



**Figure 6.37 Real environment target area (26)**



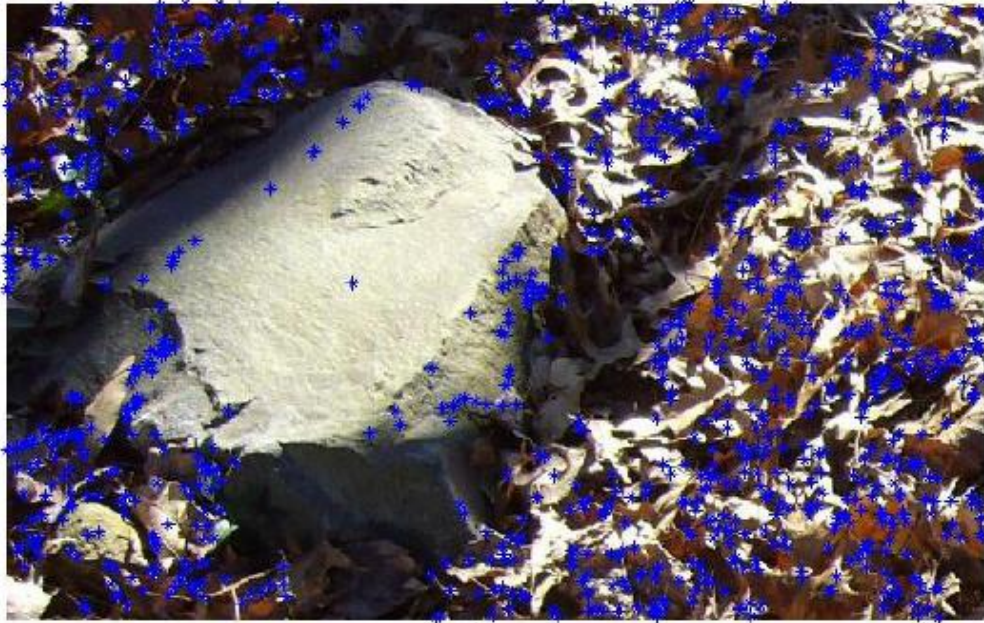


Figure 6.38 Centroid calculation for the various objects in the target area (26)

The area and centroid of the stone are calculated and the stone is automatically assumed to not be a biomass candidate based on its geometry. The leaves however pass as a biomass due to their size.

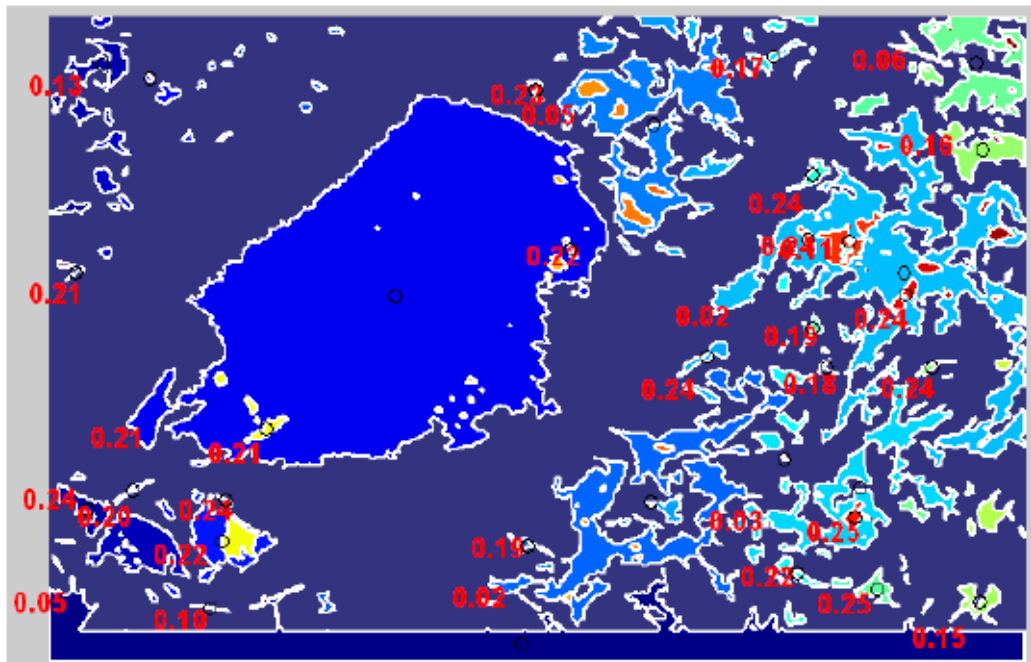


Figure 6.39 K factor calculation of the target area (26)

A more complex real time scene is now taken into consideration. Separating objects which are touching is a more complicated image processing technique. Marker-controlled watershed segmentation is used in this case. The procedure followed in this technique is (27):

1. Compute a segmentation function. This is an image whose dark regions are the objects you are trying to segment.
2. Compute foreground markers. These are connected blobs of pixels within each of the objects.
3. Compute background markers. These are pixels that are not part of any object.
4. Modify the segmentation function so that it only has minima at the foreground and background marker locations.
5. Compute the watershed transform of the modified segmentation function.



**Figure 6.40 The second real scene target area (26)**





**Figure 6.41 Gradient magnitude of the target area (26)**

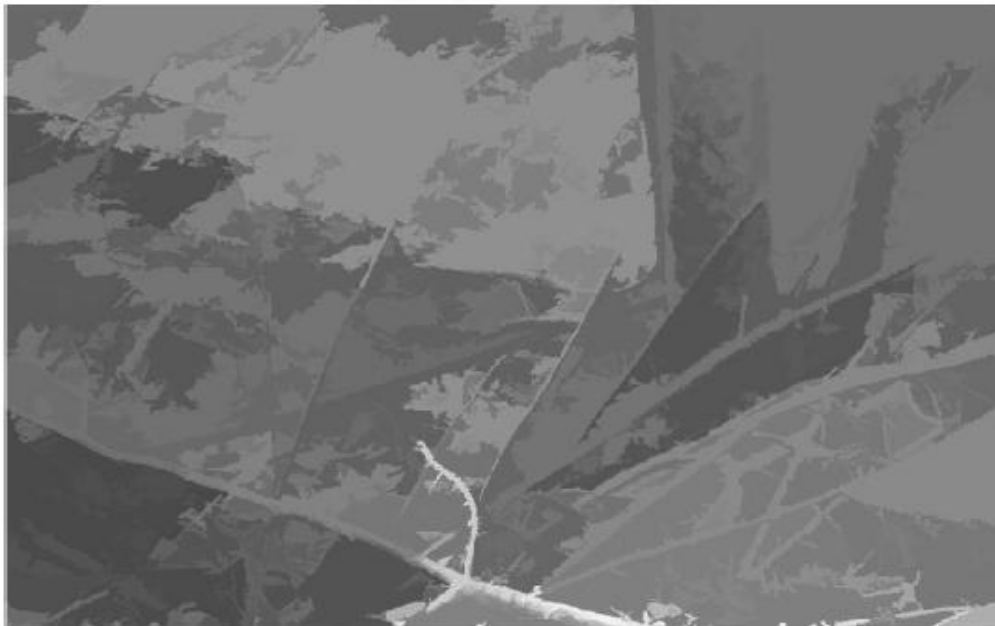


**Figure 6.42 Filtering the gradient magnitude (26)**



Figure 6.43 Watershed segmentation (26)

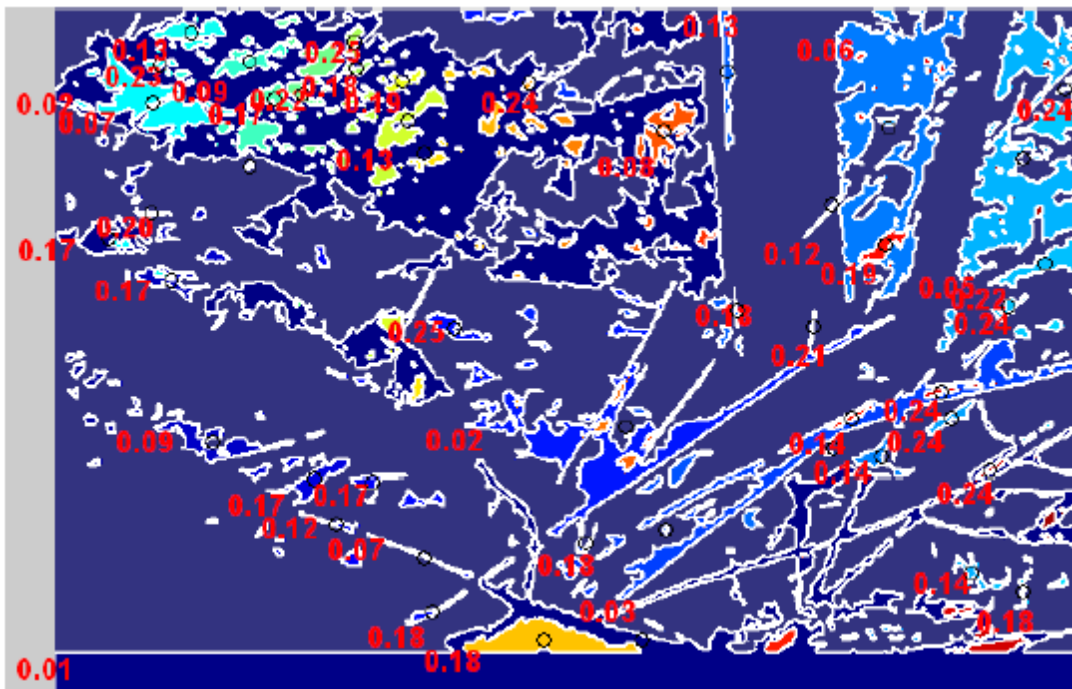


Figure 6.44 Calculating the k factors for the various objects (26)

Using the marker-controlled watershed segmentation function differentiation between connected objects is achievable. The final step is comparing the groups to the stored library of biomass properties and determining which group belongs to biomass.

## **Chapter 7: Conclusions**

The objective of this study was to develop a system capable of detecting, grasping and converting the fuel to electrical energy. Various subsystems were designed to sufficiently monitor and maintain operation. Maintaining sufficient power is essential to effectively carry out a mission. After extensive research on a slew of parts and acquisition sensors, a LADAR and webcam were chosen due to their simplicity, reliability and accuracy. The next step involved setting up an energy system capable of supplying the sensory system with adequate power. The cyclone engine and battery configuration was designed to effectively combust the biomass and keep the system running for the allotted time. A fuel moisture detection system and engine combustion controller was designed to optimize the efficiency of the combustion process. Once the energy has been converted to electricity, a battery monitor along with voltage regulators are used to effectively maintain the system power while providing the sensory system with adequate power. Testing of the system revealed that detecting objects and calculating their coordinates is not a simple task. However, after numerous tests the calculation of inverse kinematics and differentiation of biomass objects was achieved.

Real world environment test also revealed that the EATR would in fact be practical outside the laboratory.

## **Chapter 8: Future Work**

The practical end application of this project is to design a completely autonomous robot capable of performing full mission with minimal human interaction. Moving forward with this project, it is important to further optimize the configuration of the energy system. Developing a more effective technique to keep the moisture level of the biomass minimal would as well aid in maximizing the energy content of the fuel. Alternate fuels, newer battery technology and more extensive work, on the energy control systems, would be worthwhile. New technology pertaining to the various sensors should also be monitored. This would allow for the development of a more efficient and accurate sensory system. With the addition of a strain gauge to determine weight, the system will then have an additional property to correlate to prospective biomass. From a practical point of view, it has been shown that the system is capable of recognizing and obtaining required biomass. The next step from this perspective is to integrate this system on a vehicle, such as a HUMVEE, and test the real time capabilities of the integrated vehicle. Experiments in various terrains should be conducted. This allows for the collection of important data which would aid in recognizing the overall energy and mission limitations of the system. Another important step is to survey more potential environments and expand the current library for biomass definitions.

## Bibliography

1. *Autonomous Ground Vehicle Technologies Applied to the DARPA Grand Challenge*. **Carl D. Crane III, David G. Armstrong Jr, Mel W. Torrie, Sarah A. Gray**. Thailand : ICCAS, 2004.
2. Predator. *How stuff works*. [Online] [Cited: September 11, 2011.] <http://science.howstuffworks.com/predator6.htm>.
3. Predator. *How stuff works*. [Online] [Cited: September 4, 2011.] <http://science.howstuffworks.com/predator2.htm>.
4. Predator. *How stuff works*. [Online] [Cited: September 11, 2011.] <http://science.howstuffworks.com/predator3.htm>.
5. Lower and Higher Heating Values of Gas, Liquid and Solid Fuels. *Center for Transportation Analysis*. [Online] [Cited: September 18, 2011.] [http://cta.ornl.gov/bedb/appendix\\_a/Lower\\_and\\_Higher\\_Heating\\_Values\\_of\\_Gas\\_Liquid\\_and\\_Solid\\_Fuels.pdf](http://cta.ornl.gov/bedb/appendix_a/Lower_and_Higher_Heating_Values_of_Gas_Liquid_and_Solid_Fuels.pdf).
6. *Heating value of wood pellets from different sources*. **Telmo, C.** 7, s.l. : ELSEVIER, 2011, Vol. 35.
7. Battery energy storage. *All About Batteries*. [Online] [Cited: February 12, 2012.] <http://www.allaboutbatteries.com/Battery-Energy.html>.
8. **Weitkamp, Claus**. *Lidar*. Geesthacht : Springer, 2005. 0342-4111.
9. Introduction to image processing. *Space Telescope*. [Online] [Cited: December 10, 2011.] [https://www.spacetelescope.org/static/projects/fits\\_liberator/image\\_processing.pdf](https://www.spacetelescope.org/static/projects/fits_liberator/image_processing.pdf).
10. *Edge Detection Techniques for Image Segmentation- A Survey of Soft Detection Approaches*. **N. Senthilkumaran, R. Rajesh**. 2, Coimbatore : International Journal of Recent Trends in Engineering, 2009, Vol. 1.
11. The strain gauge. *Omega*. [Online] [Cited: August 24, 2011.] <http://www.omega.com/literature/transactions/volume3/strain2.html>.
12. How they work. *Sensorland*. [Online] [Cited: July 27, 2012.] <http://www.sensorland.com/HowPage047.html>.
13. humicap. *National snow and ice data center*. [Online] [Cited: July 28, 2012.] [http://nsidc.org/data/docs/daac/nsidc0008\\_hara/images/humicap.gif](http://nsidc.org/data/docs/daac/nsidc0008_hara/images/humicap.gif).
14. How to diagnose an replace. *Oxygen sensors*. [Online] [Cited: August 2, 2012.] <http://www.aalcar.com/library/o2sensor.htm>.
15. **Curkeet, Rick**. Wood Combustion Basics. *EPA*. [Online] March 2, 2011. [Cited: July 21, 2012.] <http://www.epa.gov/burnwise/workshop2011/WoodCombustion-Curkeet.pdf>.
16. Home. *Arduino*. [Online] [Cited: August 4, 2012.] <http://arduino.cc/en/>.
17. **Harry Schoell, Allan Brown, Travis Love**. *The Biomass to Power System*. Pompano Beach : Cyclone Power Technologies, 2010.
18. Wood Chipper SPEcs. *Dr Power Equipment*. [Online] [Cited: August 17, 2012.] [www.drpower/wood-chipper\\_sp\\_specs.aspx](http://www.drpower/wood-chipper_sp_specs.aspx).
19. products. *alibba*. [Online] [Cited: March 25, 2012.] [www.alibaba.com/products-gs/630200402/12v\\_50ah\\_lead\\_acid\\_battery.html](http://www.alibaba.com/products-gs/630200402/12v_50ah_lead_acid_battery.html).

20. LM2677. *Texas Instruments*. [Online] [Cited: August 12, 2011.] [www.ti.com/product/lm2677](http://www.ti.com/product/lm2677).
21. *Pellx Pellet Burner Instruction Manual*. Vittsjo : Godric Environment AB, 2010.
22. *Online monitoring of fuel moisture-content in biomass-fired furnaces by measuring relative humidity of the flue gases*. **Sven Hermansson, Frerik Lind, Henrik Thunman**. Goteborg : ELSEVIER, 2011, Vol. 89.
23. Silica Gel. *Dessicant City*. [Online] [Cited: August 26, 2012.] [http://www.agmcontainer.com/desiccantcity/desiccant\\_faqs.htm](http://www.agmcontainer.com/desiccantcity/desiccant_faqs.htm).
24. Small dehumidifiers. *B&H*. [Online] [Cited: August 16, 2012.] [http://www.bhphotovideo.com/c/product/738704-REG/Eva\\_Dry\\_EDV\\_2200\\_EDV\\_2200\\_Electric\\_Petite\\_Dehumidifier.html](http://www.bhphotovideo.com/c/product/738704-REG/Eva_Dry_EDV_2200_EDV_2200_Electric_Petite_Dehumidifier.html).
25. **Konde, Spence**. *Preparation of High-Silica Zeolite*. Worchester : s.n., 2007.
26. **Tikhonov, Nikoly**. s.l. : Robotic Technology, Inc., 2008.
27. Documentaiton center. *Mathworks*. [Online] [Cited: May 14, 2012.] [www.mathworks.com/help/images/examples/marker-controlled-watershed-segmentation.htm](http://www.mathworks.com/help/images/examples/marker-controlled-watershed-segmentation.htm).
28. Marker-Controlled Watershed Segmentation. *Mathworks*. [Online] [Cited: March 19, 2012.] <http://www.mathworks.com/help/images/examples/marker-controlled-watershed-segmentation.html>.